Gondwana Research 24 (2013) 815–837

Contents lists available at ScienceDirect

Gondwana Research

journal homepage: www.elsevier.com/locate/gr

Thermo-mechanical controls on intra-plate deformation and the role of plume-folding interactions in continental topography

S. Cloetingh [a,*], E. Burov [b,c], T. Francois [b,c]

[a] Department of Earth Sciences, Utrecht University, Budapestlaan 4, 3584 CD Utrecht, The Netherlands
[b] UPMC Sorbonne Universités, ISTEP UMR 7193, Université Pierre et Marie Curie, F-75005, Paris, France
[c] CNRS, ISTEP, UMR 7193, F-75005, Paris, France

ARTICLE INFO

Article history:
Received 24 May 2012
Received in revised form 23 November 2012
Accepted 24 November 2012
Available online 8 January 2013

Keywords:
Intraplate deformation
Lithosphere folding
Plume lithosphere interaction
Continental topography

ABSTRACT

Thermo-tectonic age and inherited structure exert the main controls on the bulk strength of the lithosphere in intraplate settings. Mechanical decoupling within the lithosphere strongly affects the interaction between deep Earth and surface processes. Thermo-mechanical models demonstrate the particular importance of the rheological stratification of the lithosphere in the preservation of ancient cratonic blocks, in the surface expression of plume- and mantle lithosphere interactions and their impact on the "dynamic" topography in general. The same is true for the effect of large-scale lithospheric folding on intraplate basin formation and associated differential vertical motions. Initiation of continental lithosphere subduction, crucial for linking orogenic deformation to intraplate deformation, appears to be facilitated by plume–lithosphere interactions. We present a discussion of these aspects, focusing on better process- understanding of continental deformation, in the context of a number of well-documented cases of intraplate deformation.

1. Introduction

The continental plates exhibit large variations of mechanical strength, as attested by numerous flexural studies (Watts, 2001; Audet and Bürgmann, 2011; Burov, 2011; Tesauro et al., 2012a). The young or thermally reset plates are mechanically weak indicating almost no resistance to tectonic loading (Watts, 2001). The oldest plates, cratons, have maximal, end-member integrated strength that is usually evoked as a key to the explanation of their preservation for billions of years. Indeed, cratons should have exceptional strength since they moved all around the Earth's surface but remained largely intact, surviving multiple plate reorganizations that led to destruction or essential reworking of the rest of the lithosphere (Francois et al., in press). In some cases, old lithosphere has been fragmented by plume events and major thermal events, such as Neoproterozoic and Phanerozoic thermal rejuvenation (e.g., the Gamburtsev Mountain Range; Ferraccioli et al., 2011), or marginally destroyed on its edges due to lateral heat exchanges and density gradients (e.g., the North China craton: Xu, 2001; Griffin et al., 2003; Bleeker, 2003). It appears that a number of cratonic plate interiors have been affected by upper mantle perturbations (Missenard et al., 2006), sometimes in interplay with reactivation by tectonic stresses and dynamical effects of subduction (Mitrovica et al, 1989), leading to a record of vertical motions deviating from models for stable platforms (e.g. Allen and Davies, 2007; Ghorbal et al., 2008). These findings point to a primary control of the thermal state, or the so-called thermo-tectonic age on the mechanical strength of the lithosphere.

Although the mechanisms controlling the mechanical strength and behavior of continental plates are not well understood, it is agreed that the following features should be of primary importance: (a) seismic thickness (H_s, ~150–350 km) defined as a layer of distinctly faster than average seismic velocities (by 1.5–2%) in global *S*-velocity tomographic models (Gung et al., 2003; Cooper and Conrad, 2009), or depth of lithosphere–asthenosphere boundary (LAB) (Rychert and Shearer, 2009; Fischer et al., 2010); (b) the degree of buoyancy of lithosphere mantle (Jordan, 1981; Doin et al., 1997; MacKenzie and Canil, 1999; Shapiro et al., 1999; Poudjom Djomani et al., 2001), basically related to its thermal state and the degree of chemical depletion; (c) the thermal state as factor impacting, as mentioned, buoyancy and the rheological strength and eventually related to surface heat flux (30–50 mW/m^2) (Mareschal and Jaupart, 2004; Jaupart and Mareschal, 2007; Lévy et al., 2010; Lévy and Jaupart, 2011) and thermal thickness, H_t, of the lithosphere; (d) integrated mechanical strength, generally evaluated from flexural isostasy studies (McKenzie and Fairhead, 1997; Watts, 2001; Audet and Bürgmann, 2011), controlled by rheological composition and many other factors; (e) litho-rheological structure of the crust and mantle lithosphere, related to the two above mentioned factors and controlling the degree of the mechanical coupling between different rheological layers, and hence the effective flexural strength and the capacity of the crust to deform together or separately from the mantle and/or to flow laterally, accommodating a part of surface loading including that related to surface erosion and sedimentation (Avouac and Burov, 1996).

* Corresponding author.
E-mail address: sierd.cloetingh@uu.nl (S. Cloetingh).

1342-937X/$ – see front matter
http://dx.doi.org/10.1016/j.gr.2012.11.012

One of the key characteristics of continental lithospheric plates, specifically old ones, has so far been insufficiently explored: the presence and preservation of the intra-crustal heterogeneities inherited from their active earlier history and nowadays acting as important internal normal loading (Cloetingh et al., 2005, 2006; Cloetingh and Ziegler, 2007). In some regions (Burov et al., 2007; Francois et al., in press) these internal loads refer to substantial heterogeneities such as frozen roots of eroded mountains or large-Moho-offset thrust faults that nowadays have no or little topographic expression, suggesting high integrated strength of the supporting mantle lithosphere.

In this paper, we explore the consequences of rheological inheritance for intraplate deformation with particular emphasis on large-scale deformation such as resulting from mantle–lithosphere interactions (MLI) or tectonic folding. We explore the consequences for the tectonics of sedimentary basin formation and thermal evolution impacting formation of natural resources. Lithospheric folding is an important mode of basin formation in compressional intraplate settings (Cloetingh et al., 1999). Basins formed by lithospheric folding are characterized by distinct features in subsidence history. A comparison with extensional basins, foreland basins, intracratonic basins and pull-apart basins provides criteria for the discrimination between these modes of basin formation. These findings (Cloetingh and Burov, 2011) are important in deciphering the feed-backs between tectonics and surface processes (Cloetingh and TOPO-EUROPE Working Group, 2007; Cloetingh et al., 2009). In addition, inferences on accommodation space and thermal regime have important consequences for hydrocarbon maturity. Lithospheric folding is coupled to compressional basin and fault reactivation and, therefore, strongly affects reservoir characteristics of sedimentary basins (Cloetingh and Ziegler, 2007).

Guillou-Frottier et al. (2012) investigated the impact of plume-lithosphere interactions (PLI) on thermo-mechanical processes affecting crustal rocks around cratonic areas. Their study was motivated by the spatial distribution of distinct types of ore deposits in east Africa, near the Tanzanian craton, and by the apparent asymmetrical behavior that seems to occur between one side of the craton and the other, as suggested by geochemical signatures of erupted lavas (Chakrabarti et al., 2009). In this context, geological, thermobarometric and metallogenic data around cratonic areas, and in particular around the Tanzanian craton were compared with the results of MLI models. Their study showed that continuous plume activity may result in partial erosion of the base of cratonic blocks, either focusing plume pathways along the sloping base of the blocks or stopping plume heads at cratonic borders. In the first case (the plume rises below the craton), favorable conditions for partial melting, ultrahigh temperature metamorphism and granite-related (tin) deposits may be established at the cratonic borders affected by downsagging (drip-like instabilities) caused by concentration of contaminated plume material flowing from under beneath the craton to the cratonic boundary. According to these models, gemstones, eclogites and ultra-high pressure metamorphism favorably occur in cases where the plume rises below a normal lithosphere, just near the lithosphere-craton boundary. The drip-like near-border instabilities result in counterclockwise P–T–t paths of the exhumed rocks, whereas slab-like instabilities are associated with clockwise P–T–t exhumation paths (Guillou-Frottier et al., 2012).

As shown by Burov and Cloetingh (2009), mantle-lithosphere interaction and folding are often superimposed in intraplate settings and the time-scales for both are controlled by the thermo-rheological structure of the lithosphere (Burov, 2011), with important consequences for the development of sedimentary basins and natural resources.

2. Rheology of continental lithosphere

Slow-deformation experimental rock mechanics data (Fig. 1; Ranalli, 1995) and flexural studies (Fig. 2, Fig. 1 in Supplementary Item E) are major, however until now not defining sources of quantitative information on the long-term behavior and strength of the lithosphere. In structured *viscous–elastic–plastic* (VEP) media, all rheological properties are inter-related, and various time- and scale-dependent factors cause variations in the effective elastic, brittle and ductile deformation. In difference from oceanic lithosphere, the continental lithosphere is mechanically stratified, consisting of many layers of contrasting rheological properties. In addition, thickness and rheological composition of different plates, specifically of their crusts (Figs. 2–4; in Supplementary Item E) may be different, thus explaining the absence of a clear correlation between the thermal age and the integrated strength of the continental lithosphere that is well observed in the oceans.

As mentioned, the main proxy to the integrated long-term strength of the lithosphere is its equivalent elastic thickness, T_e, derived from studies of flexural isostasy (e.g., Forsyth, 1985; McNutt et al., 1988; Audet and Bürgmann, 2011; Burov, 2011; Watts, 2001, Fig. 2, Fig. 1 in Supplementary Item). These studies demonstrate that the integrated strength of continental plates varies within large limits (Audet and Bürgmann, 2011, Fig. 2), highlighting the cratons as the strongest plates in the world. T_e is generally highest in coldest plates (reflecting the fact that the thermal structure of the lithosphere (see Supplementary Item A, Figs. 1 and 2) primarily controls its rheological strength profile). The rheological interpretation of flexural observations is not straightforward since it requires additional constraints on rheological parameters of at least one of the major structural units, crust or mantle (Burov, 2011). This is also evident from a comparison of the "observed" T_e (Fig. 2) and rheologically "predicted" T_e (Fig. 2) based on rock mechanics data and data on crustal thickness, thermal and lithological structure of the lithosphere (Tesauro et al., 2012b). This comparison shows, at least in some areas, quite large differences between the observed and predicted T_e. Hence, experimental rock mechanics cannot be solely used to infer long-term properties of the lithosphere. Part of the observed discrepancies with the observations can be attributed to the uncertainties of thermal and structural models of the lithosphere, whereas the other part stems from the uncertainties intrinsic to experimental rock mechanics. For a rock of given mineralogical composition and microstructure, the most important controlling parameters are temperature, fluid content, pressure, strain, strain-rate, strain history, grain size, fugacities of volatiles, and chemical activities of mineral components (Kohlstedt et al., 1995; Katayama et al., 1999; Katayama et al., 2005; Burgmann and Dresen, 2008; Keefner et al., 2011). Most of these parameters are poorly constrained in nature, explaining difficulties in extrapolating experimental rock mechanics data to geological conditions. These limitations have fuelled strong debates on the long-term strength of the lithosphere, including controversial evaluations of their thermal structure and equivalent elastic thickness (T_e; Watts and Burov, 2003; Burov, 2010).

At the outcome, two opposite, end-member rheological concepts have emerged, namely the "Jelly Sandwich (JS)" and "Crème Brûlée (CB)" models. In the JS model, the mantle lithosphere is strong and supports surface and buried tectonic loads, assuring mechanical and gravitational stability of the lithosphere, while the lower crust can be either strong or weak depending on composition. The JS model is based on the assumption of a cold, thick thermal lithosphere and dry olivine mantle rheology (cold thermal conditions and absence of fluids both favor rock strength). In the CB model, the lithospheric mantle is weak and strength is concentrated in the highly buoyant continental crust, which is supposed to keep afloat the entire lithosphere. This model assumes the hottest possible thermal structure and a wet olivine mantle rheology.

3. Constraining lithospheric behavior from large-scale observations and physical models

Due to the uncertainties of flexural data and difficulties with interpolation of experimental rock mechanics data to geological time

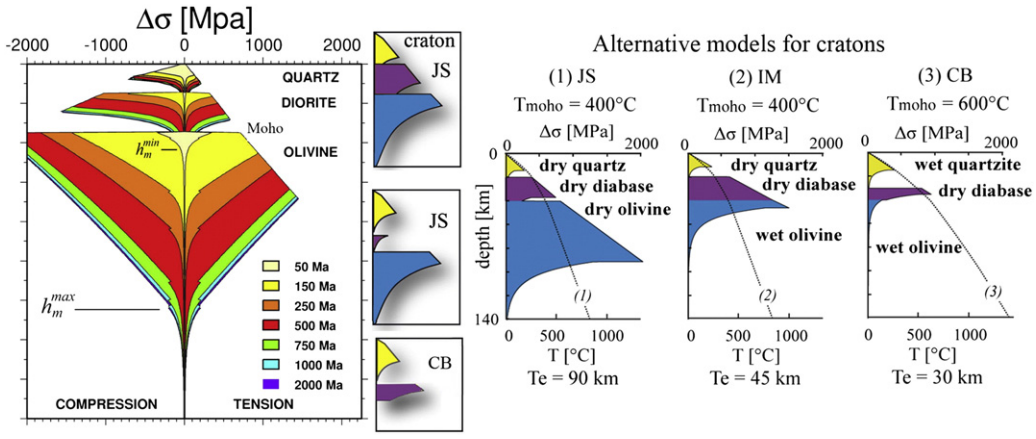

Fig. 1. Rheological models for continental lithosphere. a) Left: continental rheological yield-stress envelopes (YSE) computed for different thermo-tectonic ages (see color code) at fixed strain rate (10–15 s^{-1}). Shown in the middle (vertical column) are rheological profiles for old, normal and young lithosphere reflecting different contributions of mantle and crustal layers to the integrated strength of the plate (JS — "Jelly Sandwich"; CB — "Crème-Brulée"). Shown on the right side are three alternative rheology models for cratonic lithosphere (JS, cold, dry olivine mantle); intermediate (IM, cold, wet olivine mantle); and CB (hot, wet olivine mantle). Each envelope is shown with its corresponding equivalent elastic thickness (T_e) and geothermal profile. Color code for middle and left: yellow — upper crust; purple — lower crust; blue — mantle. It is noteworthy that rheological behavior is defined, in equal degree, by assumptions on the background geothermal profile (hence also on thermal thickness of the lithosphere) and flow-law parameters. Note also that, compared to stress limits shown in the Figure, Peierls plasticity in the mantle lithosphere may limit maximal stresses to 500–700 MPa. This will however no effect on the Te since the available flexural and tectonic stresses are unlikely to exceed 500 MPa.

scales, additional constraints are needed to understand the mechanical behavior of lithospheric plates. These additional constraints are brought by large-scale observations and physical considerations tested within self-consistent thermo-mechanical models. State-of-the-art lithosphere scale numerical thermo-mechanical models of tectonic processes account for multidisciplinary data, which allows for testing the validity of data and hypotheses on lithosphere rheology. In particular, rheological properties are particularly sensitive to various kinds of mechanical instabilities, since the growth rate of instabilities is in most cases an exponential function of the amplitude of the initial perturbation (e.g., Smith, 1979), so even modest rheology variations may have a large impact on the asymptotic behavior of the system. Here, a specific role is attributed to the gravitational–mechanical stability models that allow for straightforward tests of different thermo-rheological assumptions. This approach has also the advantage of inherent physical clearness since it is obvious that thermo-mechanical properties of geological structures should be compatible with their survival for time lapses comparable with their time spans in nature. Several types of stability tests are applied: (1) Gravitational stability of the thermo-rheological structure of the lithosphere in the absence of external forcing; (2) thermo-gravitational stability and response of the lithosphere during mantle–lithosphere interactions such as plume events; (3) response of the lithosphere to large-scale compressional tectonic forcing resulting in its folding with various observable wavelengths; and (4) by their nature, all types of instabilities may interact with each other suggesting a need for more complex models accounting for this possibility.

4. Numerical investigation of lithospheric instabilities

Lithospheric instabilities can be tested using numerical thermo-mechanical modeling approaches allowing for assessment of the mechanical response of the lithosphere in various thermo-rheological contexts. Many adequate methods can be found in literature (Schmeling et al., 2008), but we here limit our description to the one used in our previous studies. This approach is described in detail in the Supplementary item (A–D) and in earlier studies (Poliakov et al., 1993; Yamato et al., 2007; Yamato et al., 2008). Hence, we restrict the description to some essential features of the numerical technique implemented in the Flamar code based on the FLAC-Para(o)voz algorithm (Cundall, 1989; Poliakov et al., 1993, see Supplementary Item D). This thermo-mechanical code handles a free surface boundary condition that enables modeling of topography evolution, large strains and visco(ductile)-elastic-plastic(brittle) rheologies characteristic for different lithospheric and mantle units (see Tables 1, 2 and Supplementary Item B). These include Mohr–Coulomb failure for brittle deformation (faults and thrusting), pressure–temperature strain-rate dependent ductile flow for viscous deformation, thermo-dynamic phase transitions (Perple_X 2006 (Connolly, 2005)) and internal heat sources. The algorithm has no intrinsic limitations for treating physical instabilities (see Cundall, 1989) and incorporates particle-in-cell remeshing and tracking of particles. For the numerical experiments, we use the same model setup shown in Fig. 3. The multilayered visco-elasto-plastic continental lithosphere is composed of a 40 km-thick free upper-boundary crust, of which the top 20 km upper crustal layer has a dry granite rheology underlain by a 20 km-thick dry diabase lower crust. The total thickness of the lithosphere is 150 km for the CB rheology model and 250 km for the JS rheology model. The densities are updated dynamically as a function of pressure and temperature using the thermo-dynamic free-energy minimization (Connolly, 2005). The adopted temperature at the base of the upper mantle is 1700 °C, which corresponds to the assumption of whole mantle convection (Burov and Cloetingh, 2009). The initial thermal gradient in the lithosphere is computed as function of its thermo-tectonic age using a half-space cooling model (Parsons and Sclater, 1977; Burov and Diament, 1995, 1996) with account for radiogenic heat sources. The initial temperature at the base of the lithosphere is 1330 °C and the initial linear thermal gradient in the underlying mantle is such that the temperature at 650 km depth is 1700 °C (Schubert et al., 2001). Zero thermal out-flux is used as lateral boundary condition. The mechanical boundary conditions are the following: free upper surface, reflecting boundary conditions or horizontal velocities at the lateral borders, hydrostatically compensated bottom.

5. Gravitational instabilities and thermo-rheological structure of the lithosphere

The "normal" chemically undepleted mantle lithosphere is negatively buoyant so that any perturbation of major density interfaces such as the LAB results in Rayleigh-Taylor (RT) instabilities leading to destruction of the lithosphere by "de-blobbing" of the lithospheric mantle

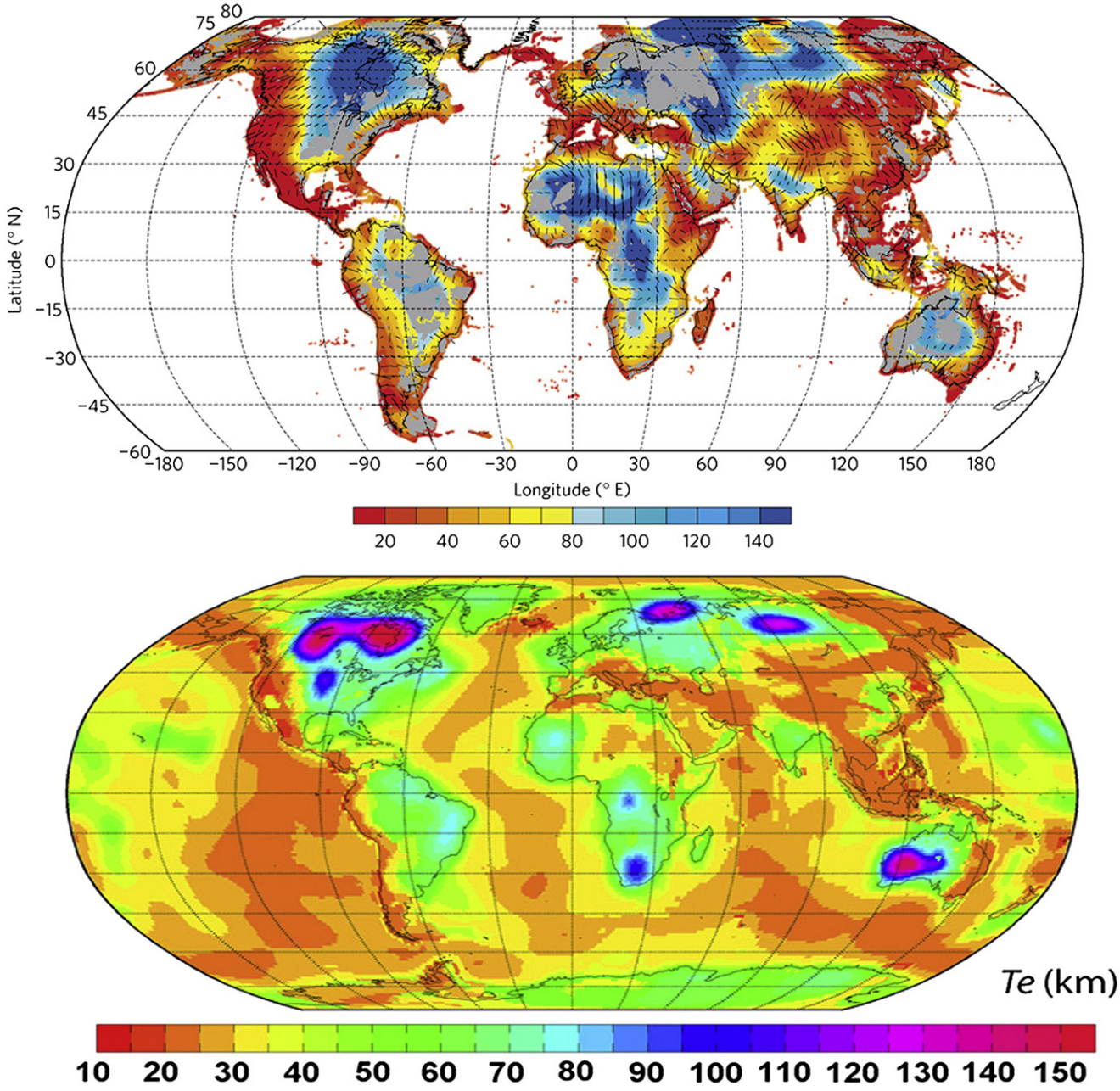

Fig. 2. Estimated T_e (bottom) based on rheological models (Tesauro et al., 2012a) compared to the "observed" T_e (top) computed from isostatic models (Audet and Bürgmann, 2011). Even though rheological interpretation of flexural observations is not straightforward, a clear match exists for many areas (Tesauro et al., 2012b) suggesting that thermo-rheological models can provide a first order approximation of the lithospheric strength.

"keels" identified with the LAB (Houseman and Molnar, 1997; Burov and Watts, 2006). Even in the case of a very strong old (i.e., $T_e > 90$–110 km (Burov and Watts, 2006)) negatively buoyant mantle lithosphere, the development of an RT instability takes a few hundreds of millions of years at most. In purely viscous lithosphere, this process cannot be slowed down to time scales larger than 300–400 Ma (Burov and Watts, 2006) and certainly not to time scales compatible with the lifespan of cratons, without reversing the density contrast between the lithosphere and asthenosphere. Beuchert et al. (2010) have demonstrated, however, that account for visco-elastic properties can increase the life-time span of negatively buoyant lithosphere under stagnant lid conditions. Nevertheless, the presence of dense heterogeneities and external tectonic forces in real-life cratons leads to deflection of the Moho and LAB boundary in the case of weak mantle lithosphere (Burov et al., 1998; Francois et al., in press), which leads to development of RT instabilities in the case of negatively buoyant mantle. Positive buoyancy of cratonic mantle (Forte and Perry, 2000; Kopylova and Russell, 2000) is thus a key factor for the longevity of cratons. Yet, as mentioned, even buoyant lithosphere may only be unconditionally stable under the "stagnant lid" condition (Solomatov, 1995; Solomatov and Moresi, 2000), i.e. when it has a horizontally homogeneous flat-layered structure not subjected to far-field tectonic forces, while the upper mantle convection parameters (such as the Rayleigh number) are tuned to prevent convective erosion of the LAB (Beuchert et al., 2010, see also below). In nature, cratons are laterally heterogeneous, bordered by thinner "normal" lithosphere of contrasting density and may be subjected to far-field forces. If preserved lithospheric plates such as cratons were not strong enough, external forces, thermal and pressure gradients resulting from lateral variations in crustal thickness and density would result in significant perturbations of density and rheological interfaces

Table 1
Thermo-mechanical coefficients and boundary conditions used in the models (Byerlee, 1978; Ranalli, 1995; Turcotte and Schubert, 2002).

Thermal	Surface temperature	0 °C
	Temperature at the bottom of the thermal lithosphere	1330 °C
	Thermal conductivity of crust	2.5 W m^{-1} °C
	Thermal conductivity of mantle	3.5 W m^{-1} °C
	Thermal diffusivity of mantle	10^{-6} m^2 s^{-1} °C
	Radiogenic heat production at surface	1×10^{-9} W kg^{-1}
	Radiogenic heat production decay depth constant	10 km
	Thermo-tectonic age of the lithosphere	1000 Ma
	Surface heat flow	40 mW m^{-2}
	Mantle heat flow	15 mW m^{-2}
Mechanical	Density for all materials	$\rho = f$ (P,T) calculated using Theriak (kg m^{-3})
	Lamé elastic constant λ, G (here, λ = G)	30 GPa
	Byerlee's law — friction angle	30°
	Byerlee's law — cohesion	20 MPa

Table 2
Creep parameters used (1 — Ranalli and Murphy, 1987; 2 — Mackwell et al., 1998; 3 — Carter and Tsenn, 1987; 4 — Wilks and Carter, 1990; 5 — Chopra and Paterson, 1984).

	Composition	A	n	ΔG	Ref.
		[MPa^{-n} s^{-1}]		[KJ mol^{-1}]	
Upper crust	Dry quartzite	6.8×10^{-6}	3	156	1
	Wet quartzite	1.1×10^{-4}	4	223	2
Lower crust	Dry Maryland diabase	8 ± 4	4.7 ± 0.6	485 ± 30	2
	Dry diabase	6.3×10^{-2}	3.05	276	3
Mantle	Dry olivine	1×10^{4}	3	520	4
	Wet olivine	417	4.48	498	5

(such as surface, LAB and Moho). Gravitational spreading, RT and marginal instabilities will develop at internal density interfaces, while perturbations and the LAB will also be eroded by convective instabilities in the upper mantle (Guillou-Frottier and Jaupart, 1995; Lenardic et al., 2003). Obviously, the threshold of such perturbations needs to be assessed.

5.1. Moho and surface topography evolution: key proxies for the survival of cratons

A most straightforward way to discriminate between end-member thermo-rheological concepts for cratons is, therefore, to test their implications for craton stability using forward thermo-mechanical models. Unlike previous studies, which imposed a rigid top as upper boundary condition thus forcing the topography to be always zero, Francois et al. (in press) implemented free-surface boundary condition, which allows for analysis of stability of surface and Moho topography, in addition to that of the LAB. The possibility to track subtle variations in surface topography (>10 m) presents a prime feature of this novel approach. The second novelty for lithosphere stability analysis refers to implementation of a petrologically-consistent density structure (computed using the reference thermo-dynamic code Perple_X) (see Supplementary Item D) and explicit, high-end viscous (ductile)–elastic–plastic (brittle) rheology laws in large-strain numerical formulation, instead of common viscous or viscous–pseudoplastic rheologies (Lenardic et al., 2003) or visco-elastic rheologies (Beuchert et al., 2010) used for lithosphere stability analysis.

In all experiments, the initial "model box" is 3000 km long and 600 km deep with a spatial resolution of 10×10 km (additional tests have been also done with resolution 10×5 km and 5×5 km to make sure that distribution and angles of shear bands are not significantly affected by resolution (Kaus, 2010)). The mechanical boundary conditions

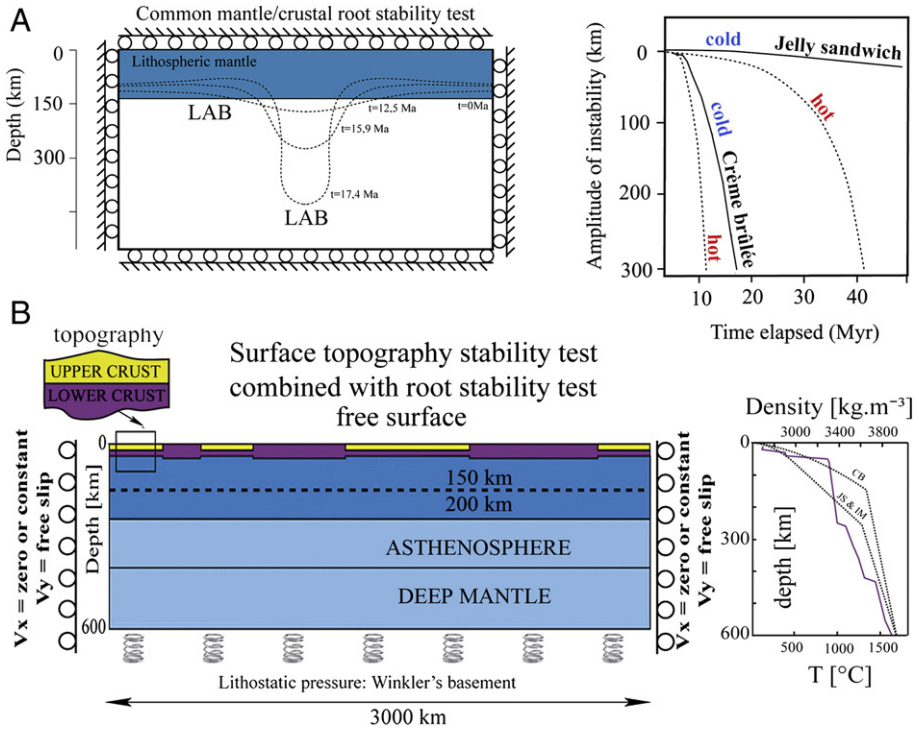

Fig. 3. Surface topography stability models. A) — Left: Conventional model for stability analysis of lithosphere (Rayleigh–Taylor instability) with negatively buoyant depleted mantle. LAB: lithosphere–asthenosphere boundary. A) — Right: Predicted amplitudes of mantle root as function of time for end-member rheological concepts (JS, "Jelly Sandwich" and CB, "Crème Brulée"). Amplitudes are computed for two end-member geotherms, "cold" and "hot" (see Burov and Watts, 2006). B) — Left: Alternative surface topography stability model for a cratonic lithosphere with positively buoyant undepleted mantle (Francois et al., in press). In difference to the conventional models, this model tests surface topography sensitivity to large lateral heterogeneities in crustal structure that are widespread in cratons. B) — Right: density profile and tested thermal structures ("hot" and "cold" corresponding to contrasting thermal models of the lithosphere behind the "CB" and "JS" rheology (Watts and Burov, 2003)). The density is computed in accordance with petrological thermodynamic data on lithosphere and mantle composition.

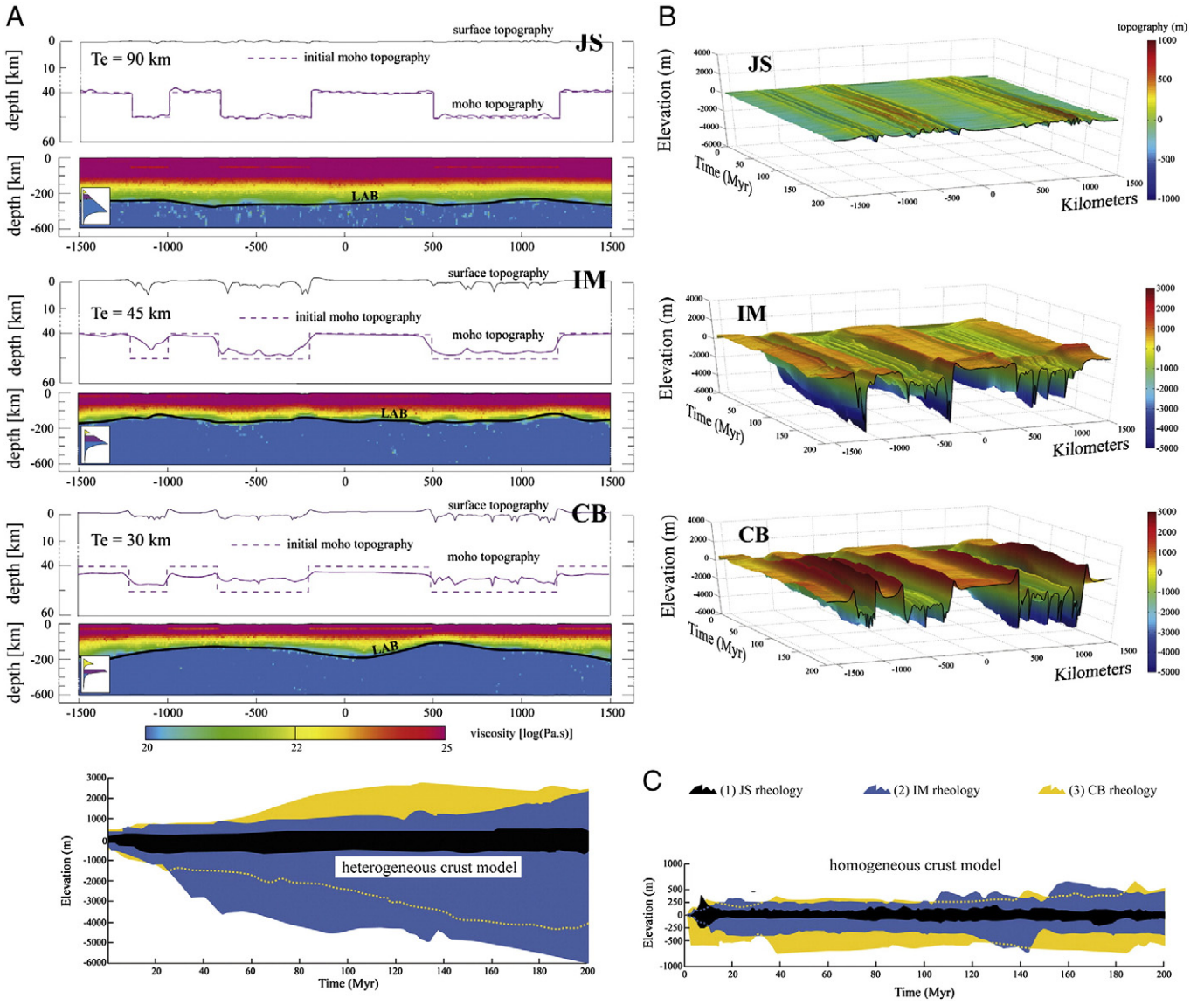

Fig. 4. Numerical experiments on craton stability corresponding to the settings shown in Fig. 3B. (A) Equivalent viscosity, surface and Moho topography evolution for three rheological assumptions: JS; CB and intermediate case (IM). (B) Predicted surface topography evolution (note that in real cratons surface topography undulations rarely exceed 100 m in the absence of strong external forcing. Hence, the JS model is most appropriate). (C) Average topography evolution as function of time (the left panel corresponds to the experiment (A)–(B) (heterogeneous crust). For comparison, the right panel shows topography evolution in case of homogeneous crust).

are as follows: (1) the upper surface is free (free stress and free slip condition in all directions); (2–3) constant horizontal velocity, v_x, at the lateral sides ($v_x = 0$ in most experiments); and (4) pliable hydrostatic Winkler basement (Burov et al., 1998; Burov and Poliakov, 2001; Burov et al., 2001). In agreement with the geological record (Flowers et al., 2006), erosion was set to zero ($k_e = 0$ m^2/yr). Thermal initial and boundary conditions vary for the different thermo-rheological scenarios considered in this study. In contrast to previous studies (Lenardic et al., 2003), the Rayleigh number of the convective mantle cannot be exactly defined because of the non-linear character of the viscosity law and dynamic phase changes (Burov et al., 2003). One can, however, estimate that Ra varies from approximately 10^7 to 0.5×10^6 in different experiments and through time, without having particular meaning. According to petrology models (Perple_X), the maximum density contrast between a completely depleted Archean mantle and the asthenosphere is on the order of 20–30 kg m^{-3}, a value corroborated by independent data on the density of mantle xenoliths (Poudjom Djomani et al., 2001). Since buoyancy favors craton stability, adoption of the maximum value of the density contrast warrants that the thermo-rheological parameters derived from our experiments correspond to the upper-bound stability range. We test the implications of the end-member rheological models: the "Jelly-Sandwich" rheology (JS; strong dry olivine mantle, strong crust, cold geotherm with Moho temperature of 400 °C and thermal lithosphere thickness of 250 km) and the "Crème Brûlée" rheology (CB; strong dry diabase lower crust, weak wet olivine mantle, Moho temperature of 600 °C and thermal lithosphere thickness of 150 km). We also tested a number of intermediate rheologies that we illustrate here with the intermediate model termed IM rheology (same rheology parameters and structure as for the CB model but a cold geotherm as for the JS model). The JS and IM cases assume the same "cold" initial geotherm based on the latest reconstruction of the thermal structure of the Canadian craton (Cooper and Conrad, 2009). The CB model relies on alternative thermal models based on the assumption of thin "hot" lithosphere (McKenzie and Fairhead, 1997; Mackwell et al., 1998; Jackson, 2002). The rheological impact of the thermal assumptions is crucial and one of the major model sensitivities: the fact that Moho temperature varies

from 400 °C to 600 °C between the JS and CB models is all-alone sufficient to produce orders of magnitude differences in the effective viscosity at Moho depths.

5.2. Confronting data and models: strong sensitivity of the predicted surface and Moho topographies to thermo-rheological assumptions

The first set of experiments shown here explores conditions of the stagnant lid approximation, i.e., a flat layered homogeneous lithosphere structure in the absence of far-field forces. The second set explores the implications of a laterally heterogeneous crustal structure, with application to the Canadian craton. We have also run additional experiments (Francois et al., in press) for the case of the Australian craton which, in contrast to the Canadian one, undergoes tectonic intraplate compression (see also Kennett and Iaffaldano, 2013–this volume). For the Canadian craton, geometrical constraints on crustal thickness and structure come from the LITHOPROBE project and relevant studies (Burov et al., 1998; Audet and Mareschal, 2004; Mareschal and Jaupart, 2004; Hammer et al., 2010; Lévy et al., 2010; Lévy and Jaupart, 2011). For the Australian craton we used the data published in Stephenson and Lambeck (1985), Clitheroe et al. (2000) and Ford et al. (2010). In these models we use a statistically representative distribution of crustal heterogeneities with horizontal dimensions in the range of 500–700 km (i.e., granulitic bodies that mimic the crustal structure of the Canadian craton: Fig. 4). The initial Moho geometry is characterized by 10 km vertical steps below the heterogeneities, in line with present-day geophysical observations. As in previous studies (Beuchert et al., 2010) we performed experiments for as long as 700 Myr. Even though the Earth system cools during billions of years changing the conditions of the convective system, there is no need to run experiments for longer time spans, since the surface topography may not disappear without leaving a traceable stratigraphic record. In most cases the asymptotic behavior of the system became clear after the first 200 Myr. We hence show here the results for 200 Myr snapshots while the results of longer control experiments are provided in the Supplementary Items.

The first "stagnant-lid" experiments, in which buoyant cratons should be stable whatever their rheology, are used to test the internal consistency of the model. In this case the crust is laterally homogeneous, without imposed far-field tectonic forces and velocities. The experiments show that under the "stagnant lid" conditions the continental lithosphere indeed remains stable (<500 m of surface topography undulations, stable flat Moho) over large time spans (700 Myr), for all tested thermo-rheological assumptions.

In contrast, the second set of experiments, which explores the impact of a laterally heterogeneous crust in the absence of far-field tectonic forcing, shows large differences between the three thermo-rheological models (Fig. 4B). Surface topography is highly unstable both for the IM and CB rheologies (Fig. 4) with differences in topographic heights on the order of 5000–8000 m (at 200 Myr, Fig. 4), which are inconsistent with stratigraphic data for the Canadian and Australian cratons (Stephenson and Lambeck, 1985; Gale, 1992; Burgess et al., 1997, 2008). In contrast, for the JS rheology, the differences in topographic height do not exceed 200 m (Fig. 4) and remain within the observed range of topographic roughness. The Moho geometry also shows marked differences between all three models after 200 Myr (Fig. 4). For the JS model, the initially prescribed 10 km Moho steps are well preserved. For the IM model, the Moho geometry is partly preserved, but locally diverges strongly from the initial geometry. For the CB model, the initial steps are flattened to only 1–2 km after 200 Myr. The LAB shows a similar trend and is increasingly unstable from the JS to IM and CB rheology. The CB model exhibits 40–80 km LAB undulations that progressively lead to small-scale convective movements and the removal of a large portion of the mantle lithosphere. For the IM and CB models, the mantle lithosphere is thinned in a number of places by a factor of 1.5–2 after 200 Myr. Given that the growth rate of viscous instabilities is an exponential function of time (Houseman et al., 1981), this indicates that 200 Myr constitutes the maximum half-life time span of a compositionally positively buoyant CB mantle (Fig. 4). It is noteworthy that the half-life time of negatively buoyant mantle is 5 to 10 times shorter (Houseman et al., 1981; Burov and Watts, 2006), confirming the idea that compositional buoyancy is a crucial – yet not sufficient – controlling factor in the preservation of cratons (e.g., Burov and Watts, 2006).

The comparison between the models involving CB or JS rheology with a homogenous or heterogeneous crust shows that the strength of the mantle lithosphere is a major stabilizing factor both for surface topography and subsurface interfaces (i.e., Moho and LAB), while a strong crust alone is insufficient to keep topography stable over significant time spans. The experiments without far-field tectonic forces indicate that the buoyancy and strength of the strong mantle lithosphere are both necessary to allow for the long-term preservation of cratons. While the previous studies have already shown that lithospheric strength matters for cratonic stability, these experiments show that it is the sub-crustal mantle lithosphere and not the cratonic crust that plays a major role in cratonic stability (e.g., Sleep, 2003a,b; Nyblade and Sleep, 2003; Lenardic et al., 2003; Beuchert et al., 2010; Francois et al., in press).

The third set of experiments (Francois et al., in press) allows for testing the effect of horizontal tectonic forces applied to cratonic lithosphere. We investigate the impact of a small shortening rate (strain rate $= 10^{-16}$ s^{-1}, as for the Australian craton (Celerier et al., 2005)). Although the Australian craton is under the present-day regime of intra-plate compression (World Stress Map, 2007) only since the Tertiary (Lithgow-Bertelloni and Richards, 1998), the numerical experiments allow exploring the effect of compression for a longer time span of 200 Myr. For the three tested thermo-rheological models, the topographic height over the first 50 Myr remains within the range observed for the Australian craton. Yet, the CB rheology induces unrealistic surface undulations with kilometric topographic heights already after 60 Myr, reaching improbable 12 km heights after 200 Myr. By comparison, the JS and IM rheologies result in more realistic topographic heights of 4 km after 200 Myr. Importantly, maximum wavelengths for the 50 and 200 Myr old topography are also more realistic for the JS model (400–700 km that fall in the observed range for the Australian craton) than for the CB model (as small as 100–200 km, i.e. 3–4 times less than observed). The importance of vertical strength partitioning in the lithosphere is another important conclusion that can be derived from these experiments. In fact, high crustal strength alone does not "save" the craton, even for non-negligible integrated lithospheric strength ($T_e = 45$ km, IM). A strong mantle lithosphere (i.e., $T_e = 90$ km, JS) is needed to support crustal irregularities and keep surface topography, Moho and LAB stable.

We herein suggest that testing the stability and evolution of surface topography in thermo-mechanical models of geodynamic processes provides a key tool for constraining the mechanical and thermal properties of the lithosphere. These results also demonstrate the necessity to consider buried or "hidden" loads and tectonic forces whenever constraining long-term rheological properties of the Archean lithosphere. One of the most critical results of the gravity stability studies concerns the rheology of mantle lithosphere and infers that the "Jelly-Sandwich" thermo-rheological model with strong dry olivine mantle, 250–300 km thick lithosphere and 400 °C temperature at Moho depth so far better accounts for geological and geophysical observations in cratons than the "Crème-Brûlée" rheology. Our findings certainly go beyond an application to cratons, suggesting, for example, that strong dry olivine mantle lithosphere is universally needed for lithosphere stability and for most lithospheric-scale tectonic processes. In case of chemically undepleted mantle ("normal" lithosphere), a strong mantle lithosphere, rather than a strong crust, appears to be the main stabilizing factor that ensures the integrity of lithospheric plates within typical time scales of tectonic processes.

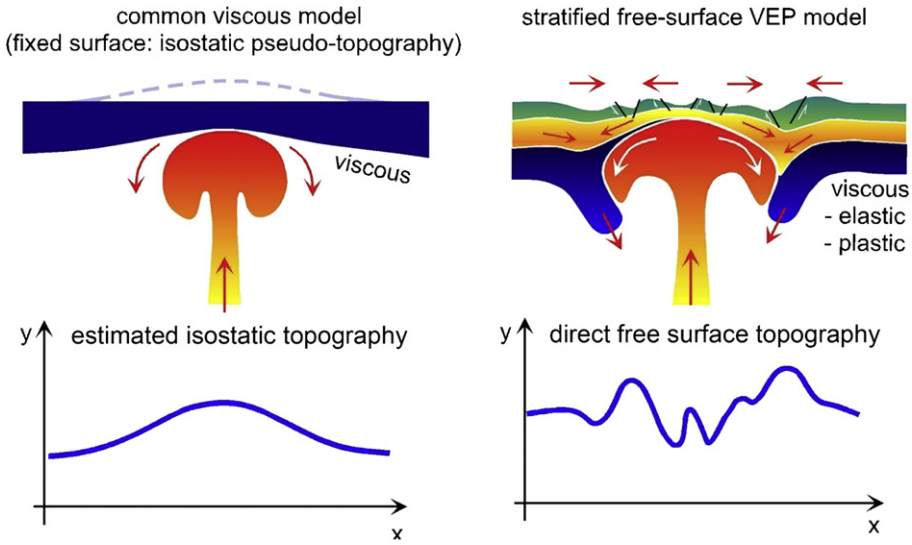

Fig. 5. Mantle–lithosphere interaction (MLI) concepts. Top left: conventional mono-layer rigid top viscous model of MLI and predicted long-wavelength dynamic topography. Top right: stratified visco-elasto-plastic (VEP) model: internal ductile layers (upper crust, green; lower crust, yellow; mantle, blue) damp plume impact and deform with their own characteristic wavelengths; mantle lithosphere can be down-thrusted in subduction-like motion.

6. Thermo-gravitational instabilities due to mantle lithosphere interactions

The physical side of the mantle plume concept includes upwelling of low density, high temperature and low viscosity mantle material separated from large-scale convective motions. When active, this upwelling is characterized by large geoid/topography ratios and can form a "superplume", i.e. a persisting diapir of a very large scale coming from the D″ boundary (e.g. Condie et al., 2000; Romanowicz and Gung, 2002), or smaller scale diapirs originating from different depths (Granet et al., 1995; Ritter et al., 2001; Courtillot et al., 2003; Montelli et al., 2004; Pilidou et al., 2005; Ritter, 2005). When convection is not chaotic, the plume tail is connected to its "mushroom" head, but when more appropriate rheologies are considered (e.g., Davies, 1994; Trompert and Hansen, 1998) the plume can ascent in a "turbulent" regime with a high ascent rate. The resulting thermo-mechanical consequences for surface geodynamics and geology appear to be largely dependent on the chosen model (structural, thermal and mechanical regimes) of the lithosphere (Burov and Guillou-Frottier, 2005; Burov et al., 2007).

This aspect has not been taken into account in many attempts to link evidence for the existence of plumes inferred from seismic tomography (e.g. Bijwaard and Spakman, 1999; Goes et al., 1999; Foulger et al., 2000; Lustrino and Carminati, 2007) to their surface expressions (e.g. White and Lovell, 1997).

The study by Burov and Guillou-Frottier (2005) was the first to pose the question on the impact of plate rheology on the dynamic topography and tectonic evolution of the lithosphere undergoing plume impingement (Fig. 5). They have shown that a conventional mono-layer rigid-top viscous model of mantle lithosphere interactions (MLI) tends to largely overestimate the wavelength of dynamic topography while omitting a wealth of consequences of MLI on surface evolution. They used instead a stratified visco-elasto-plastic model of the lithosphere with free surface topography. In doing so, they demonstrated that internal ductile layers (see Fig. 5; upper crust, green; lower crust, yellow; mantle, blue) damp plume impact and deform with their own characteristic wavelengths, whereas mantle lithosphere can be down-thrusted in subduction-like motion. These findings are corroborated by evidence from seismic tomography. Fig. 5, Supplementary Item E displays a local tomographic cross-section through the Massif Central (Koulakov et al., 2009), showing a low-velocity upper mantle anomaly below the Massif. A regional tomographic cross-section through the Pannonian basin (Fig. 5, Supplementary Item E) shows a wide anomalous upper mantle area with low seismic velocities (Wortel and Spakman, 2000).

Burov and Cloetingh (2009) performed a series of thermo-mechanically thermo-dynamically coupled numerical experiments on mantle–lithosphere interaction, consistent with an array of recent geophysical constraints on lithosphere and upper mantle rheology and structure. They demonstrated, in particular, that MLI can lead to initiation of continental lithosphere subduction, inducing its spontaneous down-thrusting to depths of 300–500 km upon plume impingement of the lithosphere. This down-thrusting is pre-conditioned by the rheological stratification of visco-elasto-plastic lithosphere (JS rheology, e.g., Toussaint et al., 2004; Gerya, 2010, 2011) and its free surface. The subsequent evolution of the slab is governed by phase changes and interactions of the downgoing slab with the surrounding mantle. It was also demonstrated that the mode of MLI is strongly affected by the lateral heterogeneities and the presence of suture zones in the lithosphere.

Dependence of the effective viscosity on depth and temperature does not allow to derive a unique Rayleigh number for a plume ascending through the upper mantle. For that we use an effective Rayleigh number for plume ascent (d'Acremont et al., 2003). We assume an ascent interval d–h and a maximal driving density contrast $\Delta\rho_{max}$, where d is the depth to the bottom of the mantle, h is the depth to the bottom of the lithosphere, $\Delta\rho_{max}=(\rho_p\alpha\Delta T_{max}+\Delta\rho_{ch})$ with ρ_p being the density of plume material at embedding temperature at depth d, and ΔT_{max} being the difference between temperatures of plume material at depths d and h. Assuming representative mean temperature T^*, a simplified approximation for the plume Rayleigh number, Ra_p, reads:

$$\begin{aligned} Ra_p &\approx g\,\Delta\rho_{max}(d-h)^3/\chi\,\mu_{eff}(r,T^*,\Delta\rho) \\ &= 3^{-(n-1)}\cdot A\cdot g^n\,\Delta\rho_{max}(r(\Delta\rho_{ch}+\alpha\rho_m\Delta T))^{n-1}(d-h)^3 \\ &\quad \div\left(\chi\cdot 6^{n-1}\cdot\exp(Q/RT^*)\right) \end{aligned}$$

where χ is the thermal diffusivity and μ_{eff} is the effective viscosity (see Supplementary items).

Instead of Ra_p, a local depth/temperature dependent Rayleigh number Ra_b can be also introduced by replacing: d–h with a diffusion length scale $\delta=(\pi\chi t_{cr})^{1/2}$; $\Delta\rho_{max}$ with $\Delta\rho$; ΔT_{max} with ΔT; and T^* with T, where t_{cr} can be found from equating R_{ab} to critical value Ra_{cr} for

onset of Rayleigh-Taylor instability ($Ra_{cr} \approx 10^3$) or by choosing some other characteristic length scale δ_l and assuming $t_{cr} = \delta_l^2/\chi$.

Compared to the case of Newtonian embeddings, Ra_p for non-Newtonian fluid (e.g., olivine, $n = 3$, Table 2) reveals a strong power-law dependence on density contrast and on plume size ($d = 2r$). For the Newtonian case, Ra_p is a linear function of the density contrast and does not depend on the plume size. In case of non-Newtonian rheology Ra_p scales as a third power of the density contrast (and thus of temperature) and as a second power of the plume size. Plume ascent through a non-Newtonian fluid is thus extremely sensitive to effective body forces. A very small variation in buoyancy forces results in strong variation in the ascent behavior (and for the final spreading below the lithosphere). For equivalent body forces, this ascent may be orders of magnitude faster than for a Newtonian fluid.

The consequences of PH–CL (plume head–continental lithosphere) interactions are mainly derived from conventional models of viscous mantle convection (e.g., Farnetani and Richards, 1994; Cserepes et al., 2000). The predictive power of these fluid dynamics models is limited because they do not adequately account for a stratified elastic–viscous–plastic lithosphere. In common convective models (e.g., Doin et al., 1997), the lithosphere is considered as a thin viscous or quasi-viscous layer with an undeformable surface. This assumption is acceptable for oceanic plates. However, as pointed out above, continental lithosphere cannot be regarded as a thin layer because its thickness (150–300 km) constitutes 50%–90% of the thickness of the convective part of the upper mantle (350–500 km). In contrast with oceanic lithosphere, the continental lithosphere is highly stratified as it is composed of a 30–70 km thick highly buoyant crust, which is quartz-rich, and a 60–250 km thick negatively or neutrally buoyant mantle layer of basic composition. The crust also counts several layers including a brittle-elastic upper crust, and a brittle–ductile–elastic middle and an elastic–ductile lower crust. Due to the presence of quartz-rich aggregates, the lower crust may have a viscosity (e.g. Kirby and Kronenberg, 1987) as low as 10^{20}–10^{21} Pa s below 15–20 km depth (250 °C–400 °C). Consequently, the high viscosity (mainly brittle) upper crust is mechanically decoupled from the strong olivine-rich lithospheric mantle, in which ductile creep is activated at high temperature (750–800 °C).

As a consequence of this decoupling, mantle deformation due to plume head impingement may produce only a moderate or strongly modulated impact on surface deformation. According to recent studies, the presence of thick stratified elastic–viscous–plastic continental lithosphere may substantially alter the surface expression of plume–lithosphere interactions (Burov and Guillou-Frottier, 2005; Burov et al., 2007; Guillou-Frottier et al., 2007,Fig. 5). Indeed, conventional monolayer models of plume–lithosphere interaction predict long-wavelength deformation with dynamic surface topography of 1–1.5 km (e.g., Ribe and Christensen, 1994). This prediction stems from the assumption that vertical undulations of the lithosphere–mantle boundary are directly transmitted to the surface. This assumption is highly questionable for continents because 1.5 km vertical displacements of the mantle–lithosphere boundary can be accommodated within a 15–30 km thick ductile lower crustal layer while the other (visco–elastic or visco–elastic–plastic) layers can relax plume-related stresses over important periods of time (up to 10 Myr). Basically, with this rheological layering, surface topography does not simply replicate the topography of the mantle–lithosphere boundary. In addition, mechanical decoupling (see also Chen et al., 2013–this volume) between the crust and mantle and the dependence of bending stresses on yield stress and plate curvature result in lateral variations of integrated plate strength and tension–compression instabilities that may yield short-wavelength topography (Burov and Diament, 1992, 1995; Burov and Guillou-Frottier, 2005).

7. Compressional instabilities (large-scale folding)

Folding is a characteristic unstable deformation that may develop in stratified media with important competence contrasts, such as the lithosphere, in response to horizontal loading (Biot, 1961; Ramberg, 1961). These instabilities develop under compression or basal shear as a result of strain/stress discontinuities on the interfaces of the mechanical layers of different mechanical strength. At the initial stages of deformation, compressional instabilities lead to the appearance of periodic folds with an exponential growth rate and a dominating wavelength, λ, roughly proportional to 5–10 thicknesses of the competent core within the lithosphere, h ($h = 10$–100 km i.e. $\lambda = 50$–1000 km).

"Biot's," or linear, folding encompasses the cases where compression of the lithosphere takes place from the beginning, leading to the formation of alternating basins and highs, and where the conditions of the linear theory are more or less satisfied (thin layer approximation, no strain-softening, plane layers, etc.). In the case of linear folding in a Newtonian media, an asymptotic relation derived from the thin layer equilibrium equation is quite simple (Biot, 1961; Ramberg, 1961):

$$\lambda_1 = 2\pi h(\mu_{l1}/6\mu_{l2})^{1/3}.$$

Here λ_l is the "Laplacian" dominant wavelength of folding in the absence of gravity, h is the thickness of the competent layer (crustal or mantle), and μ_{l1} and μ_{l2} are the effective viscosities (or competencies) of the strong layer and weak surrounds, respectively. The above equation, derived assuming no gravity, gives estimates of $\lambda_l/h = 20$–40 for typical competence contrasts. This does not hold for most lithospheric-scale cases, where $\lambda/h = 4$–6 is more common due to the influence of the gravity-dependent terms. In a simplest case of a single stiff viscous layer embedded in an inviscid medium, the dominant gravity-dependent harmonics can be accounted as (e.g., Burov and Molnar, 1998):

$$\lambda_g \sim 2\pi(2h\dot{\varepsilon}\mu eff/\Delta\rho g)^{1/2},$$

where $\Delta\rho$ is the density contrast, $\dot{\varepsilon}$ is the strain rate, μ_{eff} is the effective ductile viscosity (see Supplementary items), n is the power law exponent, and h is the thickness of the competent layer.

At large amounts of shortening this deformation may become aperiodic (e.g., Hunt et al., 1996) so that the wavelength and amplitude of folding start to vary along the deformed transect. The mentioned plume-induced periodical deformations actually also refer to folding or boudinage caused by basal shear at the bottom of the lithosphere. However, the other major reason for folding of continental lithosphere refers to tectonic loading by horizontal far-field forces (Cloetingh et al., 1999).

7.1. Plume-folding interferences

Taking into account the possibly periodical character of an instable topographic response to plume impingement, it appears that this response may effectively interfere with the periodic instable response of the lithosphere in case of its large-scale folding provoked by horizontal tectonic loading (e.g. Burov et al., 1993; Cloetingh et al., 1999; Gerbault et al., 1999). Since the folding and PLI should produce similar wavelengths of deformation, one can suggest that interaction between the two processes may result both in strong amplification or attenuation of the deformation, depending on the eventual phase shift between the wavelengths produced by folding and PLI.

7.2. Model setup for plume–lithosphere interactions (PLI)

Parametric studies by Burov and Guillou-Frottier (2005), Burov et al. (2007) and d'Acremont et al. (2003) have considered plume–continental lithosphere interactions for various visco-elastic-plastic lithospheric structures, plume head sizes and Rayleigh numbers.

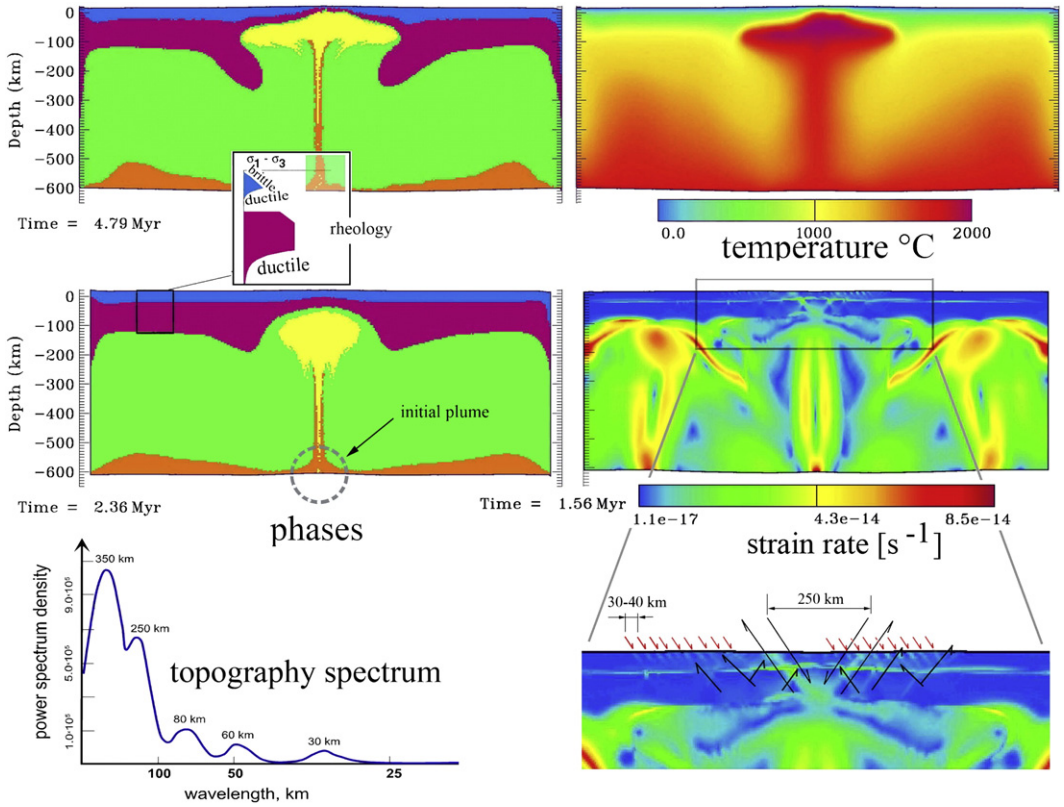

Fig. 6. MLI models: Experiment for MLI below a laterally homogeneous strong 300 Ma old continental plate. Color code: purple — mantle lithosphere, blue — upper and lower crust, green — deep mantle, yellow — plume, orange — bottom marker layer. Left: temperature field. Bottom left insert: predicted topography wavelengths. Bottom right: typical surface and crustal fault distributions associated with MLI produced in the experiment (shown field: logarithm of strain rate). Horizontal-to-vertical scale ratio equals 1 for all figures.

This experience can be combined with the results of earlier studies of lithospheric folding (Burov et al., 1993; Cloetingh et al., 1999; Gerbault et al., 1999; Cloetingh and Burov, 2011). We apply the approach based on the numerical code derived from the FLAC algorithm mentioned in the previous sections (Cundall, 1989; Poliakov et al., 1993; see also Supplementary Items C, D).

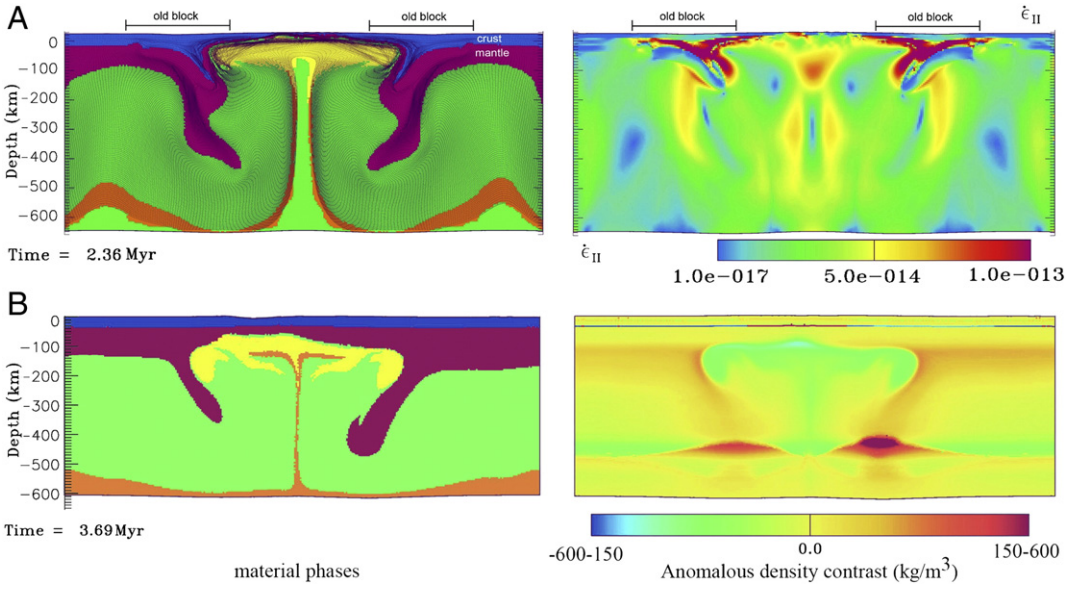

Fig. 7. MLI and initiation of subduction. (A) Experiment for MLI below a laterally heterogeneous plate that includes 300 Ma old (strong) 300 km long , 200 km thick blocks embedded in thinner (150 km) and younger (150 Ma) lithosphere. Left: phase field and passive marker grid that allows us to visualize zones of large and small deformation. Right: Strain rate field showing plug-like entrainment of the mantle lithosphere and strong deformation in the crustal parts. (B) Experiment with a plume ascending under the boundary (suture) between two continental plates of different age and thickness (150 and 300 Ma old, 150 km and 200 km, respectively). Left: material phase field. Right: Anomalous density distribution computed from phase changes (deviation from mean petrologic density similar to that inferable from the GERM/PREM seismological reference model). Positive anomalies correspond to excess density compared to the average density for the given depth. Once initialized, mantle lithosphere down-thrusting becomes a self-sustaining process. The horizontal scale of the models is identical to the vertical scale.

7.3. Plume model geometries

The development of folding and mantle plume-like instabilities has been treated in models (Figs. 6 and 7) that include lithospheric plates of various thermo-tectonic age experiencing horizontal shortening and different rates, from slow to rather fast (1.5, 3 and 6 cm/yr). Following previous plume models (e.g., Ribe and Christensen, 1994), we skip the initial (deep mantle) stages of plume rise, as they are of minor importance for near-surface evolution. In the experiments, the initial mantle plume is located at the base of the model box, and has a diameter of 100 or 200 km. We have chosen a circular shape for the initial plume because translating viscous bodies take spherical shape in laminar regime at important distance from the surface (Batchelor, 1967). This assumption corresponds to the middle mantle conditions. Nevertheless, since the model plume head is deformable, the choice of its initial geometry is of minor importance. The vertical size of the model is 650 km (upper mantle), its horizontal size is 1800 km (Fig. 6).

In the first set of experiments, the lithosphere undergoes compression without a plume at the base of the model. In the second set of experiments, the plume rises below a simultaneously compressed lithosphere. In the third set, the plume is initialized during later stages of compression, when prominent folding of the lithosphere is already observed.

7.4. Density and rheological structure of plume–lithosphere interaction models

Each element of the numerical grid is assigned its specific material phase defined as a subset of physical parameters of the corresponding material: density, thermal and EVP rheology parameters (Tables 1, 2). We use a conventional density and rheology structure for the mantle and lithosphere (Turcotte and Schubert, 2002, Fig. 6). All models include a 40 km thick crust and four horizontal rheological layers (Tables 1, 2; Kirby and Kronenberg, 1987; Carter and Tsenn, 1987): (1) a 20 km thick granite upper crust with a density of 2700 kg/m^3; (2) a 20 km thick granite lower crust with a density of 2900 kg/m^3; (3) a 60 or 160 km thick olivine mantle lithosphere with density of 3330 kg/m^3; (4) the reference mantle density at the bottom of the lithosphere is $\rho_m = 3330$ kg/m^3 (Turcotte and Schubert, 2002). The density of the plume has the same dependence on pressure as the background, so the absolute values of the background density are not important. A uniform numerical grid provides a vertical and horizontal resolution of 5 km/element (Figs. 6 and 7). The lithosphere counts 30 to 50 elements in vertical cross-section, which provides 10–15 times higher resolution than common plume models (e.g. Ribe and Christensen, 1994).

7.5. Boundary and initial conditions

As in the above described models of gravitational instabilities, zero outflow is assumed as lateral thermal condition on both sides of the box. The surface and bottom temperature is fixed at 0 °C and 2000 °C, respectively. The initial background geotherm is obtained by joining the continental and deep mantle (adiabatic) geotherms. The initial age-dependent geotherms in the lithosphere are computed according to Parsons and Sclater (1977) and Burov and Diament (1995). The lithospheric geotherm becomes adiabatic (approx. 0.3 °C/km, Sleep, 2003a,b) at depths below 1330 °C; the temperature slowly increases from 1330 °C to 1400 °C at 400 km depth, to 2000 °C at 650 km depth (e.g. Ribe and Christensen, 1994). The peculiarities of the initial geotherms in the mantle domain are of no importance because the temperature field is re-computed at each time step and the buoyancy forces are re-adjusted according to the actual and not reference thermal distribution. Since the thermal structure of lithospheric plates becomes nearly-stationary after reaching the age of 400–500 Ma (e.g. Burov and Diament, 1996), and does not practically change after 700 Ma, the maximal tested age of the lithosphere is 1000 Ma.

The mechanical boundary conditions assigned to the four sides of the box are: at the left and right sides, horizontal shortening velocity, v_x (free slip in vertical direction, free stress in all directions); at the bottom, hydrostatic pressure is applied with free slip in all directions; the surface is entirely free (free stress and free slip condition in all directions) and is affected by moderate diffusion erosion ($k = 500$ m^2/yr).

8. Experiments on plume instability

8.1. Plume instability below the continental lithosphere, in the absence of far-field compression

We first show a series of experiments with a single ($d = 200$-km) plume, upwelling below a lithosphere of constant or spatially varying (several plates) thermo-tectonic age (Figs. 6 and 7). In all these experiments we naturally use JS type rheology since, as shown by previous experiments, this is the only rheology providing sufficient conditions for long-term stability and down-thrusting of the lithosphere.

Fig. 6 (Burov and Cloetingh, 2010) shows the experiments of PLI in case of middle-aged (300 Ma and 150 Ma) lithosphere assuming a quartz-dominated rheology for the entire crust. These experiments show that an ascending plume head first (time < 1 Myr) produces large scale ($\lambda > 1000$ km) and relatively small amplitude a ($a < 1$ km) uplift superimposed on short-wavelength tensional crustal instabilities ($\lambda < 50$ km, $a < 100$ m). This deformation is soon relayed (after 1 Myr) by a higher amplitude tectonic scale uplift ($\lambda = 250$–300 km, $a \sim 2$ km) superimposed on amplified short-wavelength crustal deformation ($\lambda < 50$ km, $a \sim 300$ m). The localized topography growth continues for the next several Myr yielding final amplitudes on the order of 5 km. As its spreads laterally, the plume head erodes quite a large portion of the mantle lithosphere, provoking at 4.5–5 Myr, wholescale mantle lithosphere . At 5 Myr the crust is thinned by a factor of 3–5, yielding extreme rifting, continental break-up and onset of oceanization above the plume head. It is also noteworthy that the laterally spreading plume head laterally splits the mantle lithosphere into two parts one of which is down-thrusted, while the other thinned one remains above the plume head. At later stages, the topographic features are characterized by tectonic-scale uplift ($\lambda = 400$–500 km, $a \sim 2$ km) with smaller scale crustal wavelength.

For thermally older lithospheres (Burov and Guillou-Frottier, 2005; Burov and Cloetingh, 2009), the mantle-down-thrusting provoked by the plume head remains very important, but the amplitude of the surface expression is smaller (0.5 km) while its wavelength is larger (> 600 km). Periodic surface undulations with a wavelength of 300 km (produced by very strong crust) are also observed.

Experiments with a smaller ($d = 100$ km, Burov and Guillou-Frottier, 2005; Burov and Cloetingh, 2009) plume demonstrate that even a little "baby" plume can still have a noticeable impact on the mantle lithosphere (mantle erosion, down-thrusting) and surface topography (tectonic scale undulations with wavelengths similar to the large plume experiments and with amplitudes of up to 2000 m).

The experiments with high spatial resolution (Burov and Cloetingh, 2010, Fig. 8) on 300 Ma old lithosphere with a weak (quartz-dominated) crustal rheology show that the plume head is intruding at large scale and produces flexural scale rift shoulders. The strain rate patterns show nicely developed normal faults at the flanks of the rift. The topography has a large scale 600 km wide and 4 km high uplift. Inside the uplifted area there is a rift basin with a width of 250 km and a depth of 2 km. The flattened plume head exhibits large strain zones concentrated at the lithosphere–plume boundary. The plume continues spreading at 5.6–6 Myr. The plume moved further forward to the surface, down-thrusting subduction to 400 km and produced large wavelength uplift of an area of > 1000, with an amplitude of 4 km overlapping with a

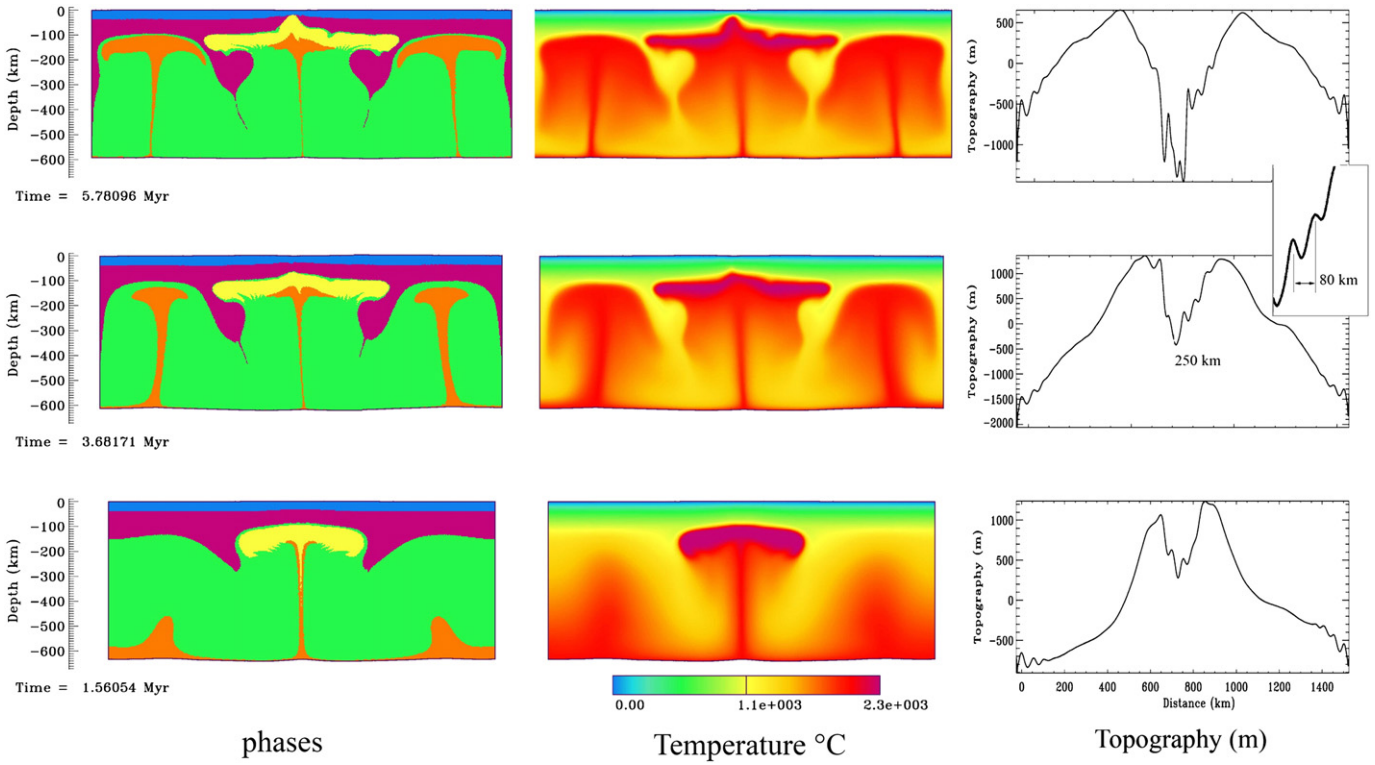

Fig. 8. High resolution experiment (2.5 km×2.5 km) with 150 Ma lithosphere (Burov and Cloetingh, 2009) showing appearance of small-scale small offset topography features related to small-scale faulting in the brittle crust (wavelengths of 30–40 km). The horizontal scale of the model is identical to the vertical scale.

small scale topography with 300 km wide area with 2 rifts, with a depth of about 2 km.

Fig. 7 demonstrates the consequences of tectonic heritage (two identical old blocks embedded in normal, i.e., younger, lithosphere). Such heterogeneities result in amplification and localization of the MLI impact so that the MLI lead to even a stronger mantle lithosphere and crustal delamination leading to large-scale subduction-like down-thrusting of the continental lithosphere on the sides of the plume head. Finally, Fig. 7B demonstrates the importance of plate boundaries showing that MLI below a boundary between two plates of contrasting age would produce a strong asymmetry in the developing mantle lithosphere instabilities, asymmetric extension at the surface and asymmetric lithosphere down-thrusting in the surrounding areas.

8.2. Folding instability in continental lithosphere in presence of far-field compression

Fig. 9a shows the poly-phase folding concept where rheological stratification results in different folding wavelengths observed at the surface. The accommodation space is created by the fold synclines while the sedimentary infill comes from the anticline folds, thus providing strong coupling between folding and basin evolution. Fig. 9b summarizes inferred cases of lithospheric folding, with the observed wavelength compared to folding wavelengths predicted by analytical models (Cloetingh et al., 1999; Burov and Cloetingh, 2009). A series of experiments investigated the development of folding instability in the lithosphere (Figs. 10–12), in the absence of mantle plumes but with the other conditions identical to the experiments of Section 7.1.

Fig. 10a shows the results of the experiments for a 250 Ma old lithosphere compressed at a slow rate of 1.25 cm/yr. In this case, some strongly decoupled low-amplitude short wavelength ($\lambda = 50$–100 km) folding superimposed on large-wavelength mantle folding (300–400 km) develops, leading to crustal thickening above synclinal mantle folds. Basically the same results were obtained for 150 Ma old lithosphere. The experiments shown in Figs. 10b and 11 put further emphasis on the effect of rheological decoupling on the observed surface topography wavelengths, specifically in case of old 500 Ma lithosphere. At large amounts of shortening, harmonic folding is relayed by mega-folding (Cloetingh et al., 1999; Burg and Podladchikov, 2000), and these mantle synclines develop in something like symmetric subduction. For lower convergence rates, folding does not develop due to the low Peclet number of the system (leading to head diffusion and weakening of folds).

Folding is well developed for medium aged and older lithospheres (>250 Ma, Figs. 10–12). In this case folding develops for all convergence rates (Burov and Cloetingh, 2009), with long mantle wavelengths ($\lambda = 300$–500 km) and high surface amplitudes (2000 m; this case corresponds to a large extend with the observed Alpine intraplate deformation of micro-continent Iberia (Cloetingh et al., 2002; De Vicente et al., 2008; Fernández-Lozano et al., 2011)). At late stages (10–26 Myr since onset of shortening for 3 cm/yr or 20–50% of shortening), folding become aperiodic leading to formation of high-amplitude crustal down-warps.

For cratonic blocks (1000 Ma old, Burov and Cloetingh, 2009), basically two wavelengths are observed ($\lambda = 150$ km and 500 km) and decoupled crustal–mantle folding occurs. The numerical experiments predict very large surface amplitudes of a 10 km scale in the case of high (6 cm/yr) convergence rates. For the intermediate (3 cm/yr) convergence rates, wavelengths are of the order of $\lambda = 560$–600 km (no crust–mantle decoupling) with amplitudes on a scale of 5 km. For the low convergence rates folding was not significant.

As mentioned, it is important that numerical thermo-mechanical models suggest that no folding occurs at very low convergence rates (<1.5 cm/yr) since at these rates gravitational instabilities take over from compressional instabilities. For high and medium convergence rates, classical high-amplitude folding is induced in intermediate (250–300 Ma) and old lithosphere (500–1000 Ma). This explains why folding develops preferably in Paleozoic massifs (e.g. Armorican Massif) or otherwise prefers pre-existing sedimentary basins (e.g. Paris Basin;

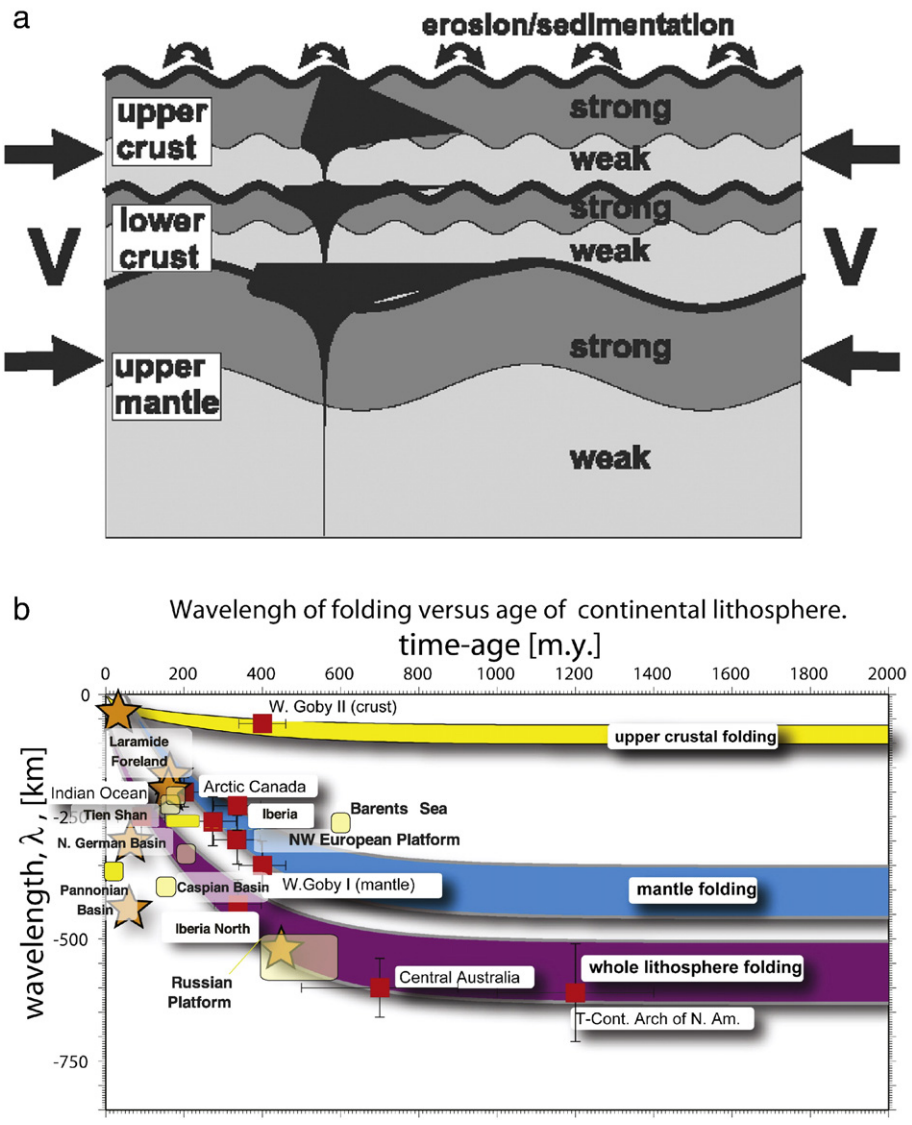

Fig. 9. Characteristics of lithospheric folding. a) Poly-harmonic folding concept: due to rheological stratification, the lithosphere can develop different folding wavelength in response to tectonic compression. Surface topography will reflect superposition of different wavelengths. b) Theoretically predicted wavelengths as function of thermo-tectonic age (for different lithospheric layers as well as whole-lithosphere folding. Model is compared to the observed wavelengths (after Cloetingh et al., 1999).

Pannonian Basin). To produce folding instabilities in young lithosphere and at low convergence rates, an interaction with plume/mantle instabilities activity is required (Burov and Cloetingh, 2009).

9. Interactions between different types of instabilities

9.1. Simultaneous plume lithosphere instabilities and folding in continental lithosphere in the presence of far field compression

In case of a very young lithosphere (60 Ma), the experiments suggest that folding can be easily overprinted by plume impact (Burov and Cloetingh, 2009).

The main differences from pure PLI deformation appear in the case of stronger lithospheres (>150 Ma) and become pronounced in case of 250–300 Ma lithosphere. In this case, surface wavelength appears to be affected by plume impact. In particular, the position of the point of maximal amplitude is shifted and one of them coincides with the presence of a plume head. The observed wavelength is $\lambda =$ 400–500 km, somewhat larger than in case of pure folding. In case of a convergence rate of 3 cm/yr, dramatic surface uplifts of 1500–2000 m with a wavelength of $\lambda = 400$ km can be observed above the top of the plume head at about 2 Myr. At later stages (5–7 Myr), the surface elevation is flattened, yielding low amplitude folding with wavelengths of $\lambda = 300$–350 km. Down-thrusting of the plume and lithosphere mantle material is well expressed in all cases.

At lower convergence rates (1.0–1.5 cm/yr), the plume produces large scale uplift with an amplitude of ~1.5 km above the plume head and a large, up to 1000 km wide area is affected by plume impingement. The initial uplift flattens out at about 8–10 Myr. Subsequently, small amplitude folding with wavelengths of $\lambda = 250$ km and small (100–300 m) vertical displacements develop. This stage might be interesting in view of subtle intraplate deformation commonly observed in intraplate settings (e.g. Siberia), traceable through river drainage patterns (Allen and Davies, 2007). Interestingly, plume material appears to be attracted by folding in Variscan-type massifs: maybe these massifs represent the optimum in terms of their rheology, which is not too strong yet but still capable to fold.

In case of strong (500–1000 Ma) lithosphere, folding develops on top of plume-induced double thrusting of crustal and upper mantle

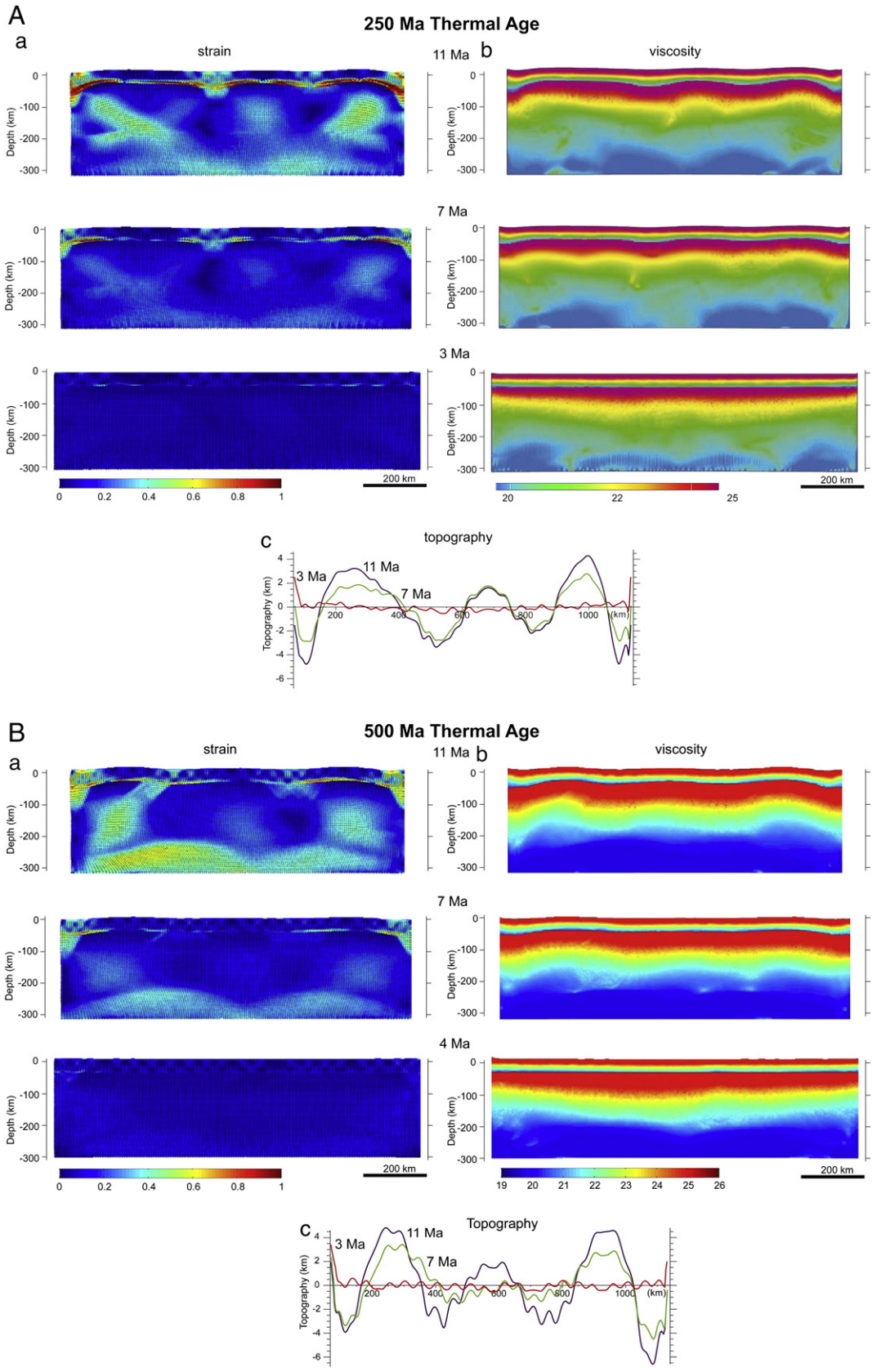

Fig. 10. Numerical model of continental folding models for thermo-tectonic ages of 250 Ma (A) and 500 Ma (B). Shown are finite strain, effective viscosity and surface topography (Smit et al., in press). Shortening at 1.25 cm/yr. The horizontal scale of the model is identical to the vertical scale.

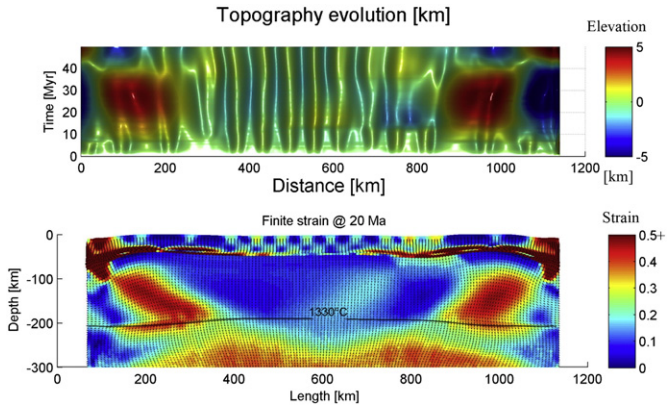

Fig. 11. Surface topography evolution at 20 Ma for the experiment shown in Fig. 10b (Smit et al., in press). The horizontal scale of the model is identical to the vertical scale.

material. However, in this case, the plume creates an initial surface uplift of about 1000 m (after 2–3 Myr) that later flattens out to smaller values of 200 m.

9.2. General characteristics of folding instabilities inferred from modeling experiments

In all folding experiments, time scales for topography creation and development are short, with rapid temporal succession from ~1000 m scale uplift caused by a plume to an 100 m scale uplift and vice versa, where in some cases large-amplitude uplift is more localized sometimes forming a mega anticline above the plume head, whereas the low amplitude surface deflection is more periodically spread over a wide area. The thermo-tectonic age of the overlying lithosphere appears to be a key factor for the temporal evolution of the surface topography: the topography pattern observed in experiments with young lithosphere (60 Ma) was exactly the opposite predicted for older ages. Although down-thrusting of mantle and plume material is well observed in the presence of tectonic compression, it is also well expressed in the experiments without compression. However, mantle down-thrusting is enhanced by compression. The experiments also show differences in the style of mantle down-thrusting: thick-skinned down-thrusting for a 60 Ma-old lithosphere versus thin-skinned down-thrusting for older lithospheres. These observations are, however, also valid for the cases without convergence.

9.3. Differences in lithosphere response to intraplate folding and PLI

The major differences between the effects of tectonically induced folding and plume activity on the lithosphere refer to (1) omni-directional, in case of homogeneous lithosphere, character of deformation produced by a plume compared to directional deformation produced by folding (this, however, is not valid if the lithosphere undergoes tectonic compression or extension at the same time as PLI); (2) folding produces significantly larger vertical amplitudes; (3) the reaction of the lithosphere to folding is instantaneous whereas there is a certain time lag (about 0.5 Myr) in case of PLI; (4) PLI induced deformation significantly varies in time, e.g. zones of surface depression may be replaced by zones of surface uplift; (5) folding requires considerable competence contrast between the lithosphere and underlying asthenosphere, i.e. folding does not develop in young continental plates.

9.4. Model diagnostics for plumes

Experiments based on a realistic plate formulation suggest that plumes and mantle instabilities can largely affect lithospheric evolution (e.g. plate break-off, extension and compression, mantle and crustal down-warping). They show that surface expressions of PLI may be quite complex (i.e., different from long-wavelength dynamic topography derived from conventional models). In particular, a plume may produce periodic zones of surface compression and extension associated with small and middle wavelengths of deformation ($\lambda = 50$, 200, 300 km … 600 km) that are commonly associated with tectonic processes.

The plume impact is most important in case of young lithosphere (<150 Ma) where it produces a series of basins and anticlines with wavelengths as small as $\lambda = 50$ km and quite large (several thousand m) vertical amplitudes. The plume impact results in removal of mantle lithosphere that is down-warped to significant depths. The crust is extended and rifted above the plume head but compression zones are also formed above the edges of the spreading plume head. As plume material flattens horizontally, it underlies the lithosphere over large

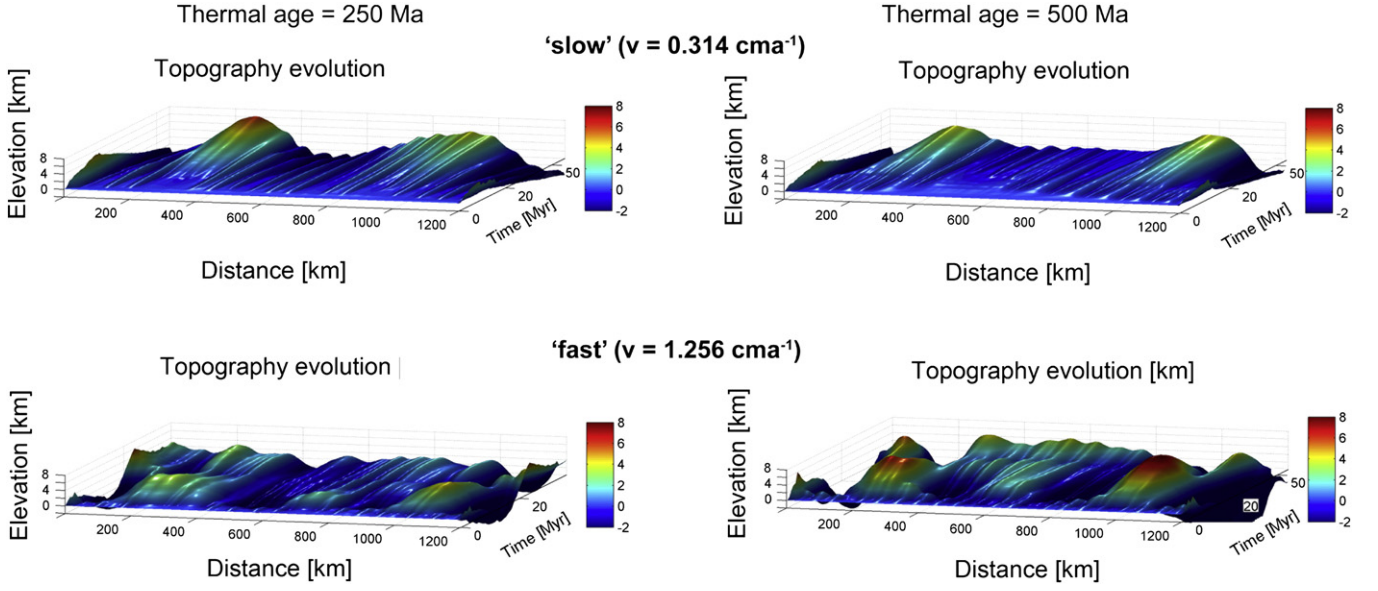

Fig. 12. Folding, effect of shortening rate. Comparison of surface topography produced by folding of the lithosphere from the experiments of Figs. 10 and 11 at different shortening rates (Smit et al., in press).

distances that exceed by a factor of 5 the initial diameter of the plume, even in cases when the plume tail is disconnected from the source region. The geodynamic influence of this material can be felt over 50–100 Myr after the plume emplacement. The predicted surface topography would be expected to possess a radial symmetry (in difference of that created by uni-directional tectonic deformation). However, the presence of inherited parallel structures within the lithosphere (e.g. series of cratonic blocks) may channelize plume head flow along their borders, resulting in directional deformation.

The plume impact is significant also for older plates, specifically for the representative 250–300 Ma lithosphere models. In this case, the produced surface wavelengths are larger and vertical amplitudes are smaller (up to 400–500 km and 1000–5000 m scale, respectively), but the overall effects are similar to the case of younger lithosphere; the plume erodes substantial quantities of lithospheric mantle resulting in a significant reduction of the integrated strength of the lithosphere. PLI with strong non-depleted old lithosphere still have very significant surface features, with wavelengths up to $\lambda = 600$–800 km and vertical uplifts in the order of several hundred meters. The bottom of the lithosphere is largely affected by plume-driven erosion and mantle downwarping that logically should result in melt infiltration from plume to the mantle lithosphere. In all cases, crust–mantle decoupling plays a very significant role for the lithospheric response during PLI. Strong decoupling reduces the effect of PLI at the surface and leads to the appearance of very small deformational wavelengths. In this case, a large part of the dynamic topography is compensated with the ductile crust.

The response of the lithosphere to a rising plume is characterized by a time lag on the order of 0.1 to 0.5 Myr and can last for tens to a hundred Myr after the plume emplacement.

9.5. Characteristics for folding inferred from model experiments

If the total amount of horizontal shortening exerted on a lithospheric plate exceeds approximately 10%, classical harmonic periodical instabilities, usually recognized as folding, may become highly aperiodic, or characterized with laterally varying wavelength. In the case of crust–mantle decoupling, folding is bi- or multi-harmonic, with generally smaller crustal wavelengths ($\lambda < 100$ km) while mantle wavelengths are in the order of $\lambda = 150$–600 km. Folding results in a drop of the integrated strength of the lithosphere at the inflection points, and thus requires a smaller force to continue after the first 10–20% of shortening are acquired. However, with time, hot material advected below anticlines cools down, whereas below a syncline cold parts of the plate get hotter. This results in a re-arrangement of the integrated strength of the plate, so that it gets stronger in ductile inflection points. The wavelength of deformation of a plate with horizontally variable strength is also variable horizontally. On the other hand, the initiated topography tends to be preserved even after cessation of tectonic forcing.

9.6. Plume-folding interactions

Plume activity followed by folding should result in strong fold amplification in the area directly affected by the plume. However, if the plate has experienced significant strength loss due to thermal re-activation by a plume, it will not fold at all due to insufficient competence contrasts with the asthenosphere.

Inversely, one can expect that folding activity followed by a thermal perturbation occurring sometime after the onset of folding may be largely perturbed in terms of the wavelength, or even interrupted (significant strength loss). The anticlines of folds would serve to catch some of the hot plume material resulting in specific spatial distribution of melting/volcanic activity.

The results of the plume-folding experiments demonstrate that plume activity facilitates folding, dramatically lowering the stresses needed for folding. Plume impact also results in the reduction of the folding wavelength and localization of folding above the plume impact area. Time is crucial in the efficiency of the interaction of plumes and folding. Lithospheric folding as a mechanism for producing thermal perturbations in the lithosphere/upper mantle system appears to be a less feasible scenario than vice versa.

As pointed out earlier, for slow convergence rates (<1.5 cm/yr) no folding in young lithosphere (<150 Ma) can be induced by far-field forces. This point is important in connection with atypical folding in some recent sedimentary basins such as the Pannonian Basin, and may serve for discrimination between expected plume and folding impact on young lithospheres.

Slow convergence promotes lithospheric mantle (and sometimes crustal) down-thrusting above plume borders and horizontal spreading of plume heads. Fast convergence enhances folding in cratonic lithospheres.

It might be important to note for the on-going discussion on the Ardennes Eiffel/Massif Central plumes (Ritter et al., 2001; Ritter, 2005; Barth et al., 2007) that classical folding inside Europe appears to be largely limited to the position of Palaeozoic massifs, including the Armorican massif (Cloetingh and Van Wees, 2005).

Plume-induced thermo-mechanical erosion of the base of young and middle aged lithospheres (<250–700 Ma, e.g., Fig. 6) appears to be a very important mechanism that may result in thinning (by factor of 2 or more) and rejuvenation of the lithosphere above the plume head over very large distances (1000 km), resulting in the formation of thin lithospheric blocks surrounded by thicker lithosphere, with deep mantle and crustal down-warping (or delamination) at the borders with the thinned areas. In compressional settings, such thinning will favor the onset of large-scale folding with variable wavelengths.

High rate shortening may prevent the development of distinct plume heads below the lithosphere. This could explain why baby plumes are observed without plume heads in domains of the intraplate lithosphere of Europe affected by compression (Gölke and Coblentz, 1996; Cloetingh et al., 2006; Jarosiński et al., 2007).

It is also likely that in case of PLI, the characteristic wavelengths of folding may not conform to the theoretical relations between thermo-mechanical age and wavelength observed for classical folding.

10. Implications for basin formation

Over the last few years much progress has been made in understanding the mechanisms of the formation of sedimentary basins in intraplate and plate-boundary settings (Cloetingh and Ziegler, 2007; Roure et al., 2010; Cloetingh and Burov, 2011). Quantitative models for several basin types have significantly advanced the understanding of extensional (McKenzie, 1978; Van Wees et al., 2009) and foreland basins (Beaumont, 1981; Naylor and Sinclair, 2008; Garcia-Castellanos and Cloetingh, 2012). The mechanisms of basin formation as a result of lithospheric folding have received considerably less attention (Cloetingh and Ziegler, 2007; Cloetingh and Burov, 2011) except for some clear-cut cases, in particular in central Asia (Burov and Molnar, 1998; Thomas et al., 1999a,b).

Many data exist on the geometry of sedimentary basins affected by large-scale compressional intraplate deformation (Cobbold et al., 1993; Lefort and Agarwal, 1996; Burov and Molnar, 1998; Lefort and Agarwal, 2000, 2002). These observations and results of analytical, numerical (Martinod and Davy, 1992; Burov et al., 1993; Gerbault et al., 1998; Cloetingh et al., 1999) and analog modeling studies (Martinod and Davy, 1994; Sokoutis et al., 2005) demonstrate that the thermo-mechanical age of the lithosphere exerts a prime control on the wavelength of lithospheric folds. These studies focused on the role of tectonic stress in lithospheric folding (Stephenson et al., 1990; Stephenson and Cloetingh, 1991; Burov and Molnar, 1998; Pérez-Gussinyé and Watts, 2005). However, as pointed out by Cloetingh and Burov (2011), surface processes also play a significant role in the mechanics of lithospheric folding. Erosion enhances the development of folding and has a

Table 3
Key characteristic features of different classes of sedimentary basins.

Basin type	Basin shape	Dimensions	Subsidence characteristics	Thermal evolution	Faulting history
FLB	Symmetrical	Width: 50–600 km; Depth: up to 20 km	Accelerated subsidence, time scales 1–10 Myr; Simultaneous uplift at highs	No initial heating; temperature increases with time with sediment deposition and burial	Intensive deformation, accelerating through basin formation phase
FB	Asymmetrical	Width: 50–250 km; Depth: up to 10 km	Linear subsidence, interrupted by short-lived faster subsidence during thrusting phases; Timescales 10–100 Myr; Simultaneous uplift from thrust front and foreland bulge	No initial heating; temperature increases with time with sediment deposition and burial	Faulting and thrusting limited to orogenic wedge; Minor deformation through faulting in foreland
EB	Symmetrical (pure shear); asymmetrical (simple shear)	Width: 30–500 km; Depth: up to 10 km	Rapid initial subsidence, followed by post-rift decay in subsidence; in case of multiple rifting repeated accelerated subsidence; Time scales for post-rift subsidence of the order of 70 Myr; At rifting stage development takes place of asymmetrical rift shoulder topography, flanking the rift	Initial heating event, followed by decaying heat flow	Extensional faulting limited to basin formation phase; During post-rift absence of faulting
PAB	Symmetrical	Width: 20–50 km; Depth: up to 10 km	Very rapid initial subsidence, followed by post-rift decay in subsidence, time scales: 1–10 Myr; In early stage, sedimentation cannot keep up with subsidence	Initial heating event, followed by very rapid decay in heat flow	Extensional faulting limited to basin formation phase; During post-rift absence of faulting
ICB	Symmetrical	Width: 500–1000 km; Depth: up to 10 km	Slow subsidence, punctuated by periods of faster subsidence, possibly related to large-scale tectonic events; Characteristic time scales: 500–800 Myr	In absence of understanding of basin formation mechanism no prediction for initial heat flow; Heat flow at later stage dominated by burial history	Very low level of faulting throughout tectonic history

pronounced effect on its wavelengths (Cloetingh et al., 1999; Burov and Toussaint, 2007), specifically in the short-wavelength domain. In addition, both sedimentation and erosion are likely to significantly prolong the lifetime of folding. Sedimentation decreases the effect of gravity by filling the downward flexed basins and thus reducing the isostatic restoring force, whereas erosion of the upward flexed basement unloads the lithosphere on the basins' uplifted flanks. Lithospheric folding has significant effects for the geometry of sedimentary sequences deposited on folded lithosphere and results in basins (FLB) with geometries, subsidence characteristics, thermal evolution and faulting histories distinctly different from other basins, including foreland basins (FB), extensional basins (EB), pull-apart basins (PAB) and intracratonic basins (ICB) (see also Table 3).

10.1. Basin shape

Folding of the lithosphere leads to a symmetrical pattern of downwarped areas (synclines) flanked by highs (anticlines) of similar amplitude and wavelength, like for instance the Ferghana basin in Central Asia (Burov and Molnar, 1998). This symmetry is in marked contrast to the asymmetrical shape of foreland basins, formed by flexure in front of an orogenic wedge, which are flanked by a flexural bulge of an amplitude that is only up to 10% of the maximum depth of the foreland depression (Royden, 1988; Zoetemeijer et al., 1999). Both types of compressional basins show a linear nature alignment of parallel depocenters and flanking highs. An important difference is the presence of parallel trending depocenters for lithospheric folding, whereas foreland flexural basins have a single depositional system. In addition, basins developed on folded lithosphere have a static location of the axis of their depocenters, in contrast to foreland basins, where the axis of depocenters can migrate with time (e.g. Zoetemeijer et al., 1993).

In both cases, the integrated strength of the lithosphere (Watts and Burov, 2003; Tesauro et al., 2007) defines the characteristic width of the basins. For folding, basin width roughly corresponds to one half of the fold wavelength (λ), which equals 5 to 10 times the thickness of the strong core of the lithospheric plate, h ($h = 10$ to 100 km, i.e. $\lambda = 50$–1000 km). In the case of crust–mantle decoupling, which occurs in relatively young plates, two dominant folding wavelengths develop (typically 250–400 km and 50–100 km). Thus two basin populations may be observed, one imbricated within the other. In the case of flexural foreland deformation, the width of the basin is controlled by the flexural parameter and is thus of the same order as the largest fold wavelength.

10.2. Subsidence patterns

Lithospheric folding results from an instability in the lithosphere due to stress/strain incompatibilities that develop in rheologically stratified layers under compressive strain. This process typically operates with timescales of the order of 1–10 Myr (Cloetingh et al., 1999). The preservation of lithospheric folds appears to depend strongly on the thermo-mechanical age of the underlying lithosphere (Cloetingh et al., 1999). Folds in young lithosphere will not be preserved upon relaxation of the stress field, whereas ones in cratonic lithosphere will be well preserved (Cloetingh et al., 1999). Fig. 13A displays characteristic basin subsidence patterns predicted by folding of 150 and 300 Ma old lithosphere due to a 3 cm/yr shortening rate. As illustrated (Fig. 13B), the differential motions occur in three distinct phases (Cloetingh and Burov, 2011):

Stage 1 is the basin formation phase, coinciding with the initiation and development of folding, which is marked by an acceleration of subsidence in the basin and uplift in the flanking highs. As a result of the time lag between sediment supply and the creation of accommodation space, during the few Myr needed to form the basin, deposition cannot keep up with subsidence causing sediment-starved basins. A similar pattern occurs in pull-apart basins (Pitman and Golovchenko, 1983) which are also associated with ultra-rapid subsidence in their formation stage also lasting only a few Myr.
Stage 2 is the basin preservation stage, where equilibrium develops between sediment supply and sediment deposition. As a result, the basin will be rapidly filled to overfilled.
Stage 3 is the basin destruction phase, characterized by basin capture and removal of sediments to areas outside the folding system. During this phase, the size of the accommodation space is reduced and erosion occurs on both flanks and depocenter. Thus, the net effect of these three stages is that lithospheric folding will lead to the development of distinct depositional–erosional cycles.

Characteristic patterns for vertical motions for folding of continental lithosphere of 150 and 300 Ma old (Fig. 13) demonstrate a remarkably

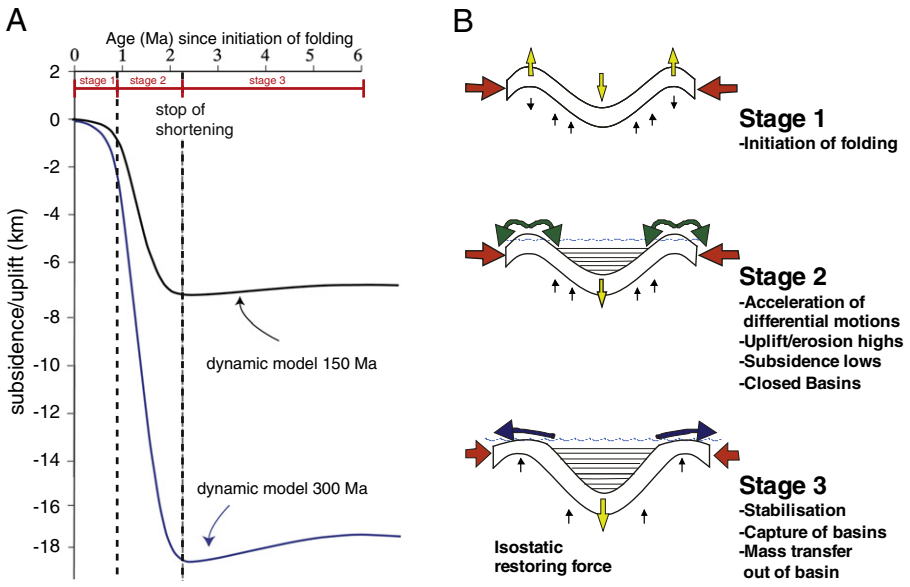

Fig. 13. (A) Characteristic subsidence patterns in the center of the synclinal depression for thermo-mechanical age of 150 and 300 Ma, respectively. Shortening rate is 3 cm/yr. (B) Characteristic stages in the evolution of a basin formed by lithospheric folding. Stage 1: Basin formation stage, acceleration of subsidence and uplift during folding. Stage 2: Steady-state: equilibrium between tectonic subsidence and sediment supply from eroding highs. Stage 3: Capture of folded basin; overall uplift and erosion. Wiggled waved blue line marks position of base level (Cloetingh and Burov, 2011).

short time scale in which substantial amounts of tectonic subsidence are induced by the process of lithospheric folding. As shown by Fig. 13, within 1 Myr after the initiation of folding induced by shortening the lithosphere at a rate of 3 cm/yr, subsidence rates are in the order of 5–15 km/Myr, depending on the thermo-mechanical age of the lithosphere. Thus, folding appears to be more effective in middle aged lithosphere of 300 Ma than in lithosphere of younger ages (Cloetingh et al., 1999; Burov and Cloetingh, 2009). After 2 Myr, a slow uplift phase starts with relatively minor magnitude of the order of a few hundreds of meters to a km. The predicted subsidence in Fig. 13 is for the center of the syncline. As pointed out above, erosion of the uplifted flanks is taken into account, adopting a diffusive equation approach to erosion (see Burov and Cloetingh, 1997; Cloetingh et al., 1999, for further details).

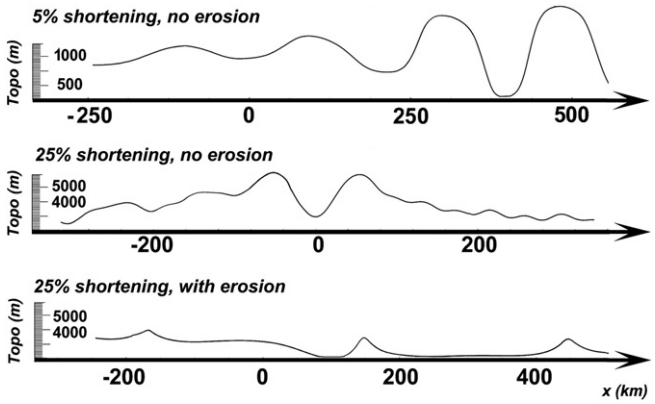

Fig. 14. Erosion and wavelength. Illustration of the effect of erosion, which acts as a filter suppressing the short wavelengths. In this case, the wavelength and amplitude vary along the cross section at different stages of deformation due to a partial crust–mantle coupling and strain localization for a 400 Ma old lithosphere with weak quartz-dominated rheology. After 5% shortening (no erosion, top), after 25% shortening (no erosion, middle), after 25% shortening (with erosion, bottom), strong zero order diffusional erosion (Avouac and Burov, 1996) tuned to keep mean elevation at the level of 3000 m. Erosion reduces the contribution of gravity-dependent terms (middle wavelength) and accelerates local deformation. Strong erosion, insufficiently compensated by the tectonic deformation wipes out most of the topography (after Cloetingh et al., 1999).

The alignment of parallel highs and basins of similar dimensions has an important consequence for the areal extent of the source areas for sediments available for deposition in the folded depressions. In comparison with foreland basins the distribution of sources is more symmetrical, superseding the volume of sediments that can be eroded from, for example, the flexural foreland bulge. As noted earlier, erosion reduces the contribution of gravity-dependent terms and accelerates local deformation. Erosion, therefore, has an important feed-back with the geometry of the accommodation space in changing the spectrum of wavelengths (Cloetingh et al., 1999). Erosion acts as a filter, suppressing the shorter wavelengths in folded basin topography. Strong erosion, insufficiently compensated by tectonic deformation, can even wipe out most of the topography. However, if the erosion is tuned to the average elevation rates (Fig. 14), it may dramatically accelerate folding (Cloetingh et al., 1999).

10.3. Marine versus continental deposits and closed basins versus capture of drainage

Erosion of uplifted areas and sedimentation in the depressions created by folded lithosphere is a self-reinforcing process promoting continuing uplift of the highs and subsidence in the depocenters. Thus, such basins will remain closed during much of their evolution. Folded basins will hence be predominantly characterized by continental deposits with only minor deposition of marine sediments during marine incursions or during basin capture. This seems to be the case for folded basins in Iberia such as the Duero Basin (Casas-Sainz and De Vicente, 2009; Fernández-Lozano et al., 2011) and Central Asia (Ferghana, Tarim Basin, Lake Issyk-Kul) (Cobbold et al., 1993). As has been pointed out for flexural foreland basins (Garcia-Castellanos et al., 2003; Garcia-Castellanos and Cloetingh, 2012), the capture time for opening basins decreases with increasing flexural rigidity. The flexural upwarp to restoring the topography removed by erosion will be almost instantaneous for very weak lithosphere, but requires up to 50–100 Myr for high lithospheric rigidities (Garcia-Castellanos et al., 2003). Thus, basins

created by folding of cratonic lithosphere probably have a shorter capture time than ones formed in younger lithosphere.

10.4. Thermal regime

Lithospheric folding is controlled by the interplay of lithospheric stresses and the inherited strength of the lithosphere. The thermal regime controls the rheological profile and differs between folded basins developed in young lithosphere and basins in cratonic lithosphere. The latter are associated with much lower thermal gradients than basins developed on young continental lithosphere. As for foreland basins, the initiation of folding is not associated with a thermal instability, unless folding occurs in conjunction with plume activity (Burov and Cloetingh, 2009). Following the deposition of radiogenic sediments in the folded depression, sediment blanketing will affect the heat flow (Stephenson et al., 1990; Lavier and Steckler, 1997; Van Wees et al., 2009), modifying the surface heat flow in the basin center. As pointed out by Lavier and Steckler (1997) and Ziegler et al. (1998), the effect of sediment fill is to weaken the lithosphere. The low thermal conductivities of the sediments lead to high temperatures in the upper lithosphere and consequently low local yield strength. During basin subsidence, sediments deposited in the central parts of the basin might be exposed to temperature windows corresponding to hydrocarbon generation. At the same time, sediments pre-dating the folding may have undergone extra burial due to syn-folding sedimentation.

During basin capture overall cooling takes place. This effect is illustrated by characteristic thermal evolution for different thermotectonic ages of 150 and 300 Ma of the folded continental lithosphere, incorporating radioactive heat production in the sediments filling in the synclinal depression, shown in Fig. 6 Supplementary Item E. Subsidence induced by folding is calculated for the center of the basin. Basins developing on folded lithosphere are characterized by their relatively low heat flow at the onset of folding, followed by a steady increase with time, doubling the heat flow over a time interval of the order of 5 Myr following the cessation of shortening. This increase is primarily due to the contribution of radioactive heat production in the very substantial pile of sediments accumulating in a relatively short time interval. The patterns of heat flow are similar for different thermo-mechanical ages of the lithosphere, with the oldest lithosphere having the lower heat flow. Older ages enhance the accommodation space and the contribution of the sediments to heat flow but are compensated by a larger decrease in heat flow with aging lithosphere. Another important factor is the mode of folding. Crustal scale folding, will be associated with shorter wavelengths, shallower basin depths and thinner sequences of heat producing sediments than for mantle lithospheric folding.

11. Discussion

As shown above, the rheological structure of the continental lithosphere has a strong impact on its evolution. The preservation of Archean cratons and of cratonized lithosphere in general and the degree to which the intraplate lithosphere is prone to folding and mantle–lithosphere interactions is very sensitive to the rheological stratification of the lithosphere.

Even if in the case of pure stagnant lid conditions the lithosphere can be preserved for billions of years irrespective of its rheological profile. However, the presence of frozen internal heterogeneities and of external forcing require high mechanical resistance of cratonic mantle lithosphere. This conclusion is particularly reinforced by models testing the stability of surface and preservation of Moho topography as function of the thermo-rheological profile.

Intraplate folding, in addition to being a basin forming mechanism, frequently interacts with other tectonic processes. As pointed out by Cloetingh (1988), intraplate compression can modify pre-existing basins. The Pannonian Basin of Central Europe created by Miocene back-arc extension appears to be an example of such a configuration, characterized by a-typical a-periodic folding (Horváth and Cloetingh, 1996; Bada et al., 1998; Horváth et al., 2006; Bada et al., 2007). Other examples are cratonic sag basins where intraplate compression (Cloetingh, 1988) is thought to occur in interaction with phase changes in the lithosphere (Artyushkov, 2007). Examples of these might be the Barents Sea (Ritzmann and Faleide, 2009) and possibly the South Caspian Basin, although in the latter case pre-orogenic extension cannot be ruled out (Guest et al., 2007). Basins exposed to changes in tectonic regime will have a polyphase record (Cloetingh and Ziegler, 2007), characterized by a superposition of more than two regimes, such as pre-orogenic extension, foreland flexure and late-stage folding. This sequence appears to be characteristic for some very deep foreland basins, such as the Focsani depression of the Romanian Carpathians, with more than 16 km of sediments, which was affected by extension due to the opening of the Black Sea Basin, followed by foreland flexure and overprinted by Late Miocene compression (Tarapoanca et al., 2003). As pointed out above (Ziegler and Dèzes, 2007), the Alpine intraplate evolution of the Northwestern European foreland reflects lithosphere folding, overprinting, rifting and foreland flexure. Quantification of the topographies created by rifting and foreland flexure and correcting for them is essential to reconstruct the shape of the additional accommodation shape created by subsequent lithospheric folding (Bourgeois et al., 2007).

The impingement of plumes on the base of continental lithosphere in intraplate settings can induce differential topography similar to the surface deflections characteristic for lithosphere folds (Burov et al., 2007; Guillou-Frottier et al., 2007). Plumes and lithospheric folds frequently interact in space and time in the geological record of intraplate areas (Ziegler and Dèzes, 2007; Burov and Cloetingh, 2009). Therefore, the evolution of folded lithosphere basins can be overprinted by the signatures of a plume or vice-versa. This will lead to an amplification of the induced vertical motions, particularly significant for young and intermediate age lithosphere. Emplacement of hot upper mantle material will raise temperatures in the lithosphere and increase heat flow. Due to the lag time in the propagation of heat, the effect at the surface might become manifest only after several tens of Myr. Plume emplacement might also weaken the lithosphere, making it more prone to intraplate compressional fault reactivation after cessation of the folding.

For continental deep Europe, an extensive data base exists to constrain the link between upper mantle structure and lithospheric processes (e.g. Artemieva et al., 2006). Interplay of lithosphere folding and plume impingement on the continental intraplate lithosphere occurred probably almost simultaneously in late Neogene times in the Northwestern European foreland. Two examples are the Eifel and Massif Central areas of the Alpine foreland of NW Europe (Dezes et al., 2004; Cloetingh and van Wees, 2005; Ziegler and Dèzes, 2007). Both areas are sites of main Late Neogene volcanic activity in the European Cenozoic rift system (ECRIS). Seismic tomography (Ritter et al., 2001) shows finger shaped baby plumes with a characteristic spatial diameter of 100 km, extending downward to 400 km. Ziegler and Dèzes (2007) proposed that plume activity occurs simultaneously with recent compressional deformation in the Massif Central area (Guillou-Frottier et al., 2007) and the Ardennes/Eifel area. Geomorphological studies constrain the recent uplift of the Ardennes and the Eifel area. An order in magnitude difference occurs between the uplift of the Eifel area, underlain by a plume and the adjacent Ardennes area where evidence for a plume is lacking. The patterns of uplift appear to be radial, superimposed by a linear NE–SW trend perpendicular to the main axis of compression. Baby plumes primarily develop in the anticlines of lithospheric folds (Burov and Cloetingh, 2009). The plume activity presumably accelerated the rate of uplift by a factor of 3–5 (Cloetingh and Ziegler, 2007). According to presently available data, the plumes in this segment of the European Cenozoic Rift System arrived about 1 Myr ago. This activity

was preceded and followed by lithospheric folding that continues to the present day since 17 Myr ago (Bourgeois et al., 2007).

Thermo-mechanical modeling illustrates the relative effectiveness of amplification of lithosphere deformation and topographic effects induced by plumes though folding and vice-versa. Burov and Cloetingh (2009) examined the response times and time-lags involved and whether these baby plumes were more efficient in localizing deformation than large plumes. Plume-affected folding appears to accelerate surface uplift, whereas folding goes into saturation and stagnates when plastic hinges form. For the discrimination of plumes and folding it is critical to access constraints on the presence or absence of radial versus linear symmetry, heat flow anomalies, gravity and geoid data. Plume activity facilitates folding, by dramatically lowering the stress levels required (Burov and Cloetingh, 2009). Plume impact also reduces the fold wavelength and localizes folding above the plume impact area. A general outcome of the modeling and observations is that lithospheric folding as a mechanism for producing thermal perturbations in the lithosphere/upper mantle system in intraplate settings is a less feasible scenario. Thermo-mechanical age and crustal structure are key controls on the stability and response of the lithosphere during MLI and horizontal tectonic forcing.

12. Conclusions

A large number of studies have addressed the mechanical structure and long-term rheology of continental lithosphere. These studies benefitted from constraints on the lithological and thermal structure of the lithosphere, findings from rock mechanics data and inferences from flexural and thermo-mechanical modeling of continental lithosphere in various tectonic settings. First order models have been developed for the present-day structure of several continents, including Europe as well as models with lower resolution of a global scale. These models suggest that thermo-rheological structure of the lithosphere (linked to its thermo-tectonic age) exerts a main control on the mode of the intraplate deformation. Continental lithosphere displays strong spatial and temporal variations, with various degrees of mechanical decoupling between crustal and mantle parts of the mechanically strong lithosphere. Thermo-mechanical models demonstrate the particular importance of the lithosphere mantle strength in the preservation of cratonic blocks. The rheological stratification of the lithosphere has also strong impact on the surface expression of plume- and mantle lithosphere interactions and its consequences for the “dynamic” topography in general. The same applies also for the effect of large-scale lithospheric folding on intraplate basin formation and associated differential vertical motions. Initiation of continental lithosphere subduction, crucial for linking orogenic deformation to intraplate deformation appears to be facilitated by plume-lithosphere interactions and also requires strong mantle lithosphere. Thermo-mechanical models and their validation with data from a number of well-documented cases of intraplate deformation provide new insights in mechanisms of continental deformation and their interrelations with deep mantle dynamics.

Supplementary data to this article can be found online at http://dx.doi.org/10.1016/j.gr.2012.11.012.

Acknowledgments

We are thankful to the anonymous reviewer and Taras Gerya for many insightful and constructive comments on the manuscript. This research has been funded through the Netherlands Research Centre for Integrated Solid Earth Science (ISES) and ISTEP (UPMC-CNRS). Dr. Fred Beekman, Jeroen Smit and Elishevah van Kooten are thanked for technical assistance.

References

Allen, M.B., Davies, C.E., 2007. Unstable Asia: active deformation of Siberia revealed by drainage shifts. Basin Research 19, 379–392.
Artemieva, I.M., 2011. The Lithosphere, an Interdisciplinary Approach. Cambridge University Press (773 pp.).
Artemieva, I.M., Thybo, H., Kaban, M.K., 2006. Deep Europe today: geophysical synthesis of the upper mantle structure and lithospheric processes over 3, 5 Ga. In: Gee, D., Stephenson, R. (Eds.), European Lithosphere Dynamics: Geological Society of London, Memoirs, 32, pp. 11–42.
Artyushkov, E.V., 2007. Formation of the superdeep Caspian Basin: subsidence driven by phase change in continental crust. Russian Geology and Geophysics 48, 1002–1014.
Audet, P., Bürgmann, R., 2011. Dominant role of tectonic inheritance in supercontinent cycles. Nature Geosciences 4, 184–187.
Audet, P., Mareschal, J.-C., 2004. Variations in elastic thickness in the Canadian Shield. Earth and Planetary Science Letters 226, 17–31.
Avouac, J.P., Burov, E.B., 1996. Erosion as a driving mechanism of intracontinental mountain growth. Journal of Geophysical Research 101, 17747–17769.
Bada, G., Cloetingh, S., Gerner, P., Horváth, F., 1998. Sources of recent tectonic stress in the Pannonian region: inferences from finite element modelling. Geophysical Journal International 134, 87–101.
Bada, G., Grenerczy, G., Tóth, L., Horváth, F., Stein, S., Cloetingh, S., Windhoffer, G., Fodor, L., Pinter, N., Fejes, I., 2007. Motion of Adria and ongoing inversion of the Pannonian basin: seismicity, GPS velocities and stress transfer. In: Stein, S., Mazzotti, S. (Eds.), Continental Intraplate Earthquakes: Science, Hazard, and Policy Issues: GSA Special Paper, 425, pp. 243–262.
Barth, A., Jordan, M., Ritter, J.R.R., 2007. Crustal and upper mantle structure of the French Massif Central plume. In: Ritter, J.R.R., Christensen, U.R. (Eds.), Mantle Plumes — A Multidisciplinary Approach. Springer Verlag, Heidelberg, pp. 159–184.
Batchelor, G.K., 1967. An Introduction to Fluid Dynamics. Cambridge University Press (615 pp.).
Beaumont, C., 1981. Foreland basins. Geophysical Journal of the Royal Astronomical Society 65, 291–329.
Beuchert, M.J., Podladchikov, Y.Y., Simon, N.S.C., Ruepke, L.H., 2010. Modeling of craton stability using a viscoelastic rheology. Journal of Geophysical Research 115, B11413.
Bijwaard, H., Spakman, W., 1999. Tomographic evidence for a narrow whole mantle plume below Iceland. Earth and Planetary Science Letters 166, 121–126.
Biot, M.A., 1961. Theory of Folding of Stratified viscoelastic media and its implications in tectonics and orogenesis. Geological Society of America Bulletin 72, 1595–1620.
Bleeker, W., 2003. The late Archean record: a puzzle in ca. 35 pieces. Lithos 71, 99–134.
Bourgeois, O., Ford, M., Diraison, M., Carlier, Le, de Veslud, C., Gerbault, M., Pik, R., Nuby, N., Bonnet, S., 2007. Separation of rifting and lithospheric folding signatures in the NW-Alpine foreland. International Journal of Earth Sciences 96, 1003–1031.
Burg, J.-P., Podladchikov, Y., 2000. From buckling to asymmetric folding of the continental lithosphere: numerical modelling and application to the Himalayan syntaxes. In: Asif Khan, M., Qasim Jan, M., Treloar, P.J., Searle, M.P. (Eds.), Tectonics of the Nanga Parbat Syntexis and the Western Himalaya and Karakoram: Geological Society of London, Special Publication, 170, pp. 219–236.
Burgess, P.M., Gurnis, M., Moresi, L., 1997. Formation of sequences in the cratonic interior of North America by interaction between mantle, eustatic and stratigraphic processes. Geological Society American Bulletin 108, 1515–1535.
Burgess, P.M., 2008. Phanerozoic evolution of the sedimentary cover of the North American craton. In: Miall, A.D. (Ed.), The Sedimentary Basins of the United States and Canada. Elsevier, Amsterdam, pp. 31–63.
Burgmann, R., Dresen, G., 2008. Rheology of the lower crust and upper mantle: evidence from rock mechanics, geodesy, and field observations. Annual Review of Earth and Planetary Sciences 36, 531–567.
Burov, E.B., 2010. The equivalent elastic thickness (Te), seismicity and the long-term rheology of continental lithosphere: time to burn-out “crème brûlée”? Insights from large-scale geodynamic modelling. Tectonophysics 484, 4–26.
Burov, E., 2011. Rheology and strength of the lithosphere. Marine and Petroleum Geology 28, 1402–1443.
Burov, E.B., Cloetingh, S., 1997. Erosion and rift dynamics: new thermo-mechanical aspects of post-rift evolution of extensional basins. Earth and Planetary Science Letters 150, 7–26.
Burov, E.B., Cloetingh, S., 2009. Controls of mantle plumes and lithospheric folding on modes of intra-plate continental tectonics: differences and similarities. Geophysical Journal International 178, 1691–1722.
Burov, E.B., Cloetingh, S., 2010. Plume-like upper mantle instabilities drive subduction initiation. Geophysical Research Letters 37, L03309.
Burov, E.B., Diament, M., 1992. Flexure of the continental lithosphere with multilayered rheology. Geophysical Journal International 109, 449–468.
Burov, E., Diament, M., 1996. The effective elastic thickness (EET) and inelastic rheology of continents and oceans. Geology 24, 419–423.
Burov, E.B., Diament, M., 1995. Effective elastic thickness of the continental lithosphere — what does it really mean? Journal of Geophysical Research 100, 3905–3927.
Burov, E.B., Guillou-Frottier, L., 2005. The plume head — continental lithosphere interaction using a tectonically realistic formulation for the lithosphere. Geophysical Journal International 161, 469–490.
Burov, E., Molnar, P., 1998. Gravity anomalies over the Ferghana Valley (central Asia), and intracontinental deformation. Journal of Geophysical Research 103, 18137–18152.
Burov, E., Poliakov, A., 2001. Erosion and rheology controls on syn- and post-rift evolution: verifying old and new ideas using a fully coupled numerical model. Journal of Geophysical Research 106, 16461–16481.

Burov, E., Toussaint, G., 2007. Surface processes and tectonics: forcing of continental subduction and deep processes. Global and Planetary Change 58, 141–164.
Burov, E.B., Watts, A.B., 2006. The long-term strength of continental lithosphere: "jelly-sandwich" or "crème-brulé"? GSA Today 16, 4–10.
Burov, E., Lobkovsky, L., Cloetingh, S., Nikishin, A., 1993. Continental lithosphere folding in Central Asia. Part 2: constraints from gravity and topography. Tectonophysics 226, 73–87.
Burov, E., Jaupart, C., Mareschal, J.-C., 1998. Large-scale crustal heterogeneities and lithospheric strength in cratons. Earth and Planetary Science Letters 164, 205–219.
Burov, E.B., Jolivet, L., Le Pourhiet, L., Poliakov, A., 2001. A thermomechanical model of exhumation of HP and UHP methamorphic rocks in Alpine mountain belts. Tectonophysics 342, 113–136.
Burov, E., Jaupart, C., Guillou-Frottier, L., 2003. Ascent and emplacement of buoyant magma bodies in brittle–ductile upper crust. Journal of Geophysical Research 108, 2177.
Burov, E., Guillou-Frottier, L., d'Acremont, E., Le Pourhiet, L., Cloetingh, S., 2007. Plume Head–lithosphere interactions near intra-continental plate boundaries. Tectonophysics 434, 15–38.
Byerlee, J.D., 1978. Friction of rocks. Pure and Applied Geophysics 116, 615–626.
Carter, N.L., Tsenn, M.C., 1987. Flow properties of continental lithosphere. Tectonophysics 36, 27–63.
Casas-Sainz, A.M., De Vicente, G., 2009. On the tectonic origin of Iberian topography. Tectonophysics 474, 214–235.
Celerier, J., Sandiford, M., Hansen, D.L., Quigley, M., 2005. Modes of active intraplate deformation, Flinders Ranges, Australia. Tectonics 24, TC6006.
Chakrabarti, R., Basu, A.R., Santo, A.P., Tedesco, D., Vaselli, O., 2009. Isotopic and geochemical evidence for a heterogeneous mantle plume origin of the Virunga volcanics, Western rift, East African Rift system. Chemical Geology 259, 273–289.
Chen, Y., Zhang, Z., Sun, C., Badal, J., 2013. Crustal anisotropy from Moho converted Ps wave splitting analysis and geodynamic implications beneath the eastern margin of Tibet and surrounding regions. Gondwana Research 24, 946–957 (this volume).
Chopra, P.N., Paterson, M.S., 1984. The role of water in the deformation of dunite. Journal of Geophysical Research 89, 7861–7876.
Clitheroe, G., Gudmundsson, O., Kennett, B.L.N., 2000. The crustal thickness of Australia. Journal of Geophysical Research 105, 697–713.
Cloetingh, S., 1988. Intraplate stresses: a new element in basin analysis. In: Kleinspehn, K.L., Paolo, C. (Eds.), New Perspectives in Basin Analysis. Springer-Verlag, NewYork, pp. 205–230.
Cloetingh, S., Burov, E.B., 2011. Lithospheric folding and sedimentary basin evolution: a review and analysis of formation mechanisms. Basin Research 23, 257–290.
Cloetingh, S.A.P.L., TOPO-EUROPE Working Group, 2007. TOPO-EUROPE: the geoscience of coupled deep Earth-surface processes. Global and Planetary Change 58, 1–118.
Cloetingh, S., Van Wees, J.D., 2005. Strength reversal in Europe's intraplate lithosphere: transition from basin inversion to lithospheric folding. Geology 33, 285–288.
Cloetingh, S., Ziegler, P.A., 2007. Tectonic models of sedimentary basins. In: Watts, A.B. (Ed.), Treatise on Geophysics, 6. Elsevier, pp. 485–611.
Cloetingh, S.A.P.L., Burov, E., Poliakov, A., 1999. Lithosphere folding: primary response to compression? (from central Asia to Paris basin). Tectonics 18, 1064–1083.
Cloetingh, S.A.P.L., Burov, E., Beekman, F., Andriessen, P.A.M., Garcia-Castellanos, D., De Vicente, G., Vegas, R., 2002. Lithospheric folding in Iberia. Tectonics 21, 1041.
Cloetingh, S.A.P.L., Ziegler, P.A., Beekman, F., Andriessen, P.A.M., Matenco, L., Bada, G., Garcia-Castellanos, D., Hardebol, N.N., Dèzes, P., Sokoutis, D., 2005. Lithospheric memory, state of stress and rheology: neotectonic controls on Europe's intraplate continental topography. Quaternary Science Reviews 24, 241–304.
Cloetingh, S., Cornu, T., Ziegler, P.A., Beekman, F., ENTEC Working Group, 2006. Neotectonics and intraplate continental topography of the northern Alpine Foreland. Earth-Science Reviews 74, 127–196.
Cloetingh, S., Thybo, H., Faccenna, C., 2009. TOPO-EUROPE: Studying continental topography and Deep Earth-Surface processes in 4D. Tectonophysics 474, 4–32.
Cobbold, P.R., Davy, P., Gapais, D., Rossello, E.A., Sadybakasov, E., Thomas, J.C., Tondji Biyo, J.J., de Urreiztieta, M., 1993. Sedimentary basins and crustal thickening. Sedimentary Geology 86, 77–89.
Condie, K.C., Des Marais, D.J., Abbott, D., 2000. Geologic evidence for a mantle superplume event at 1.9 Ga. Geochemistry, Geophysics, Geosystems 1, GC000095.
Connolly, J.A.D., 2005. Computation of phase equilibria by linear programming: a tool for geodynamic modeling and its application to subduction zone decarbonation. Earth and Planetary Science Letters 236, 524–541.
Cooper, C.M., Conrad, C.P., 2009. Does the mantle control the maximum thickness of cratons? Lithosphere 1, 67–72.
Courtillot, V., Davaille, A., Besse, J., Stock, J., 2003. Three distinct types of hotspots in the Earth's mantle. Earth and Planetary Science Letters 205, 295–308.
Cserepes, L., Christensen, U.R., Ribe, N.M., 2000. Geoid height versus topography for a plume model of the Hawaian swell. Earth and Planetary Science Letters 178, 29–38.
Cundall, P.A., 1989. Numerical experiments on localization in frictional materials. Ingenieur Archive 59, 148–159.
D'Acremont, E., Leroy, S., Burov, E.B., 2003. Numerical modelling of a mantle plume: the plume head-lithosphere interaction in the formation of an oceanic large igneous province. Earth and Planetary Science Letters 206, 379–396.
Davies, G.F., 1994. Thermomechanical erosion of the lithosphere by mantle plumes. Journal of Geophysical Research 99, 15709–15722.
De Vicente, G., Cloetingh, S., Muñoz-Martín, A., Olaiz, A., Stich, D., Vegas, R., Galindo-Zaldívar, J., Fernández-Lozano, J., 2008. Inversion of moment tensor focal mechanisms for active stresses around the Microcontinent Iberia: tectonic implications. Tectonics 27, TC1009.
Dezes, P., Schmid, S.M., Ziegler, P.M., 2004. Evolution of the European Cenozoic Rift System: interaction of the Alpine and Pyrenean orogens with their foreland lithosphere. Tectonophysics 389, 1–33.
Doin, M.-P., Fleitout, L., Christensen, U., 1997. Mantle convection and stability of depleted and undepleted continental lithosphere. Journal of Geophysical Research 102, 2771–2787.
Farnetani, C.G., Richards, M.A., 1994. Numerical investigations of the mantle plume initiation model for flood basalt events. Journal of Geophysical Research 99, 13813–13833.
Fernández-Lozano, J., Sokoutis, D., Willingshofer, E., Cloetingh, S., De Vicente, G., 2011. Cenozoic deformation of Iberia: a model for intraplate mountain building and basin development based on analogue modeling. Tectonics 30, TC1001.
Ferraccioli, F., Finn, C.A., Jordan, T.A., Bell, R.E., Anderson, L.M., Damaske, D., 2011. East Antarctic rifting triggers uplift of the Gamburtsev Mountains. Nature 479, 388–392.
Fischer, K.M., Ford, H.A., Abt, D.L., Rychert, C.A., 2010. The lithosphere–asthenosphere boundary. Annual Review of Earth and Planetary Sciences Letters 38, 551–575.
Flowers, R.M., Bowring, S.A., Reiners, P.W., 2006. Low long-term erosion rates and extreme continental stability documented by ancient (U–Th)/He dates. Geology 34, 925–928.
Ford, H.A., Fischer, K.M., Abt, D.L., Rychert, C.A., Elkins-Tanton, L.T., 2010. The lithosphere asthenosphere boundary and cratonic lithospheric layering beneath Australia from Sp wave imaging. Earth and Planetary Science Letters 300, 299–310.
Forsyth, D.W., 1985. Subsurface loading and estimates of the flexural rigidity of continental lithosphere. Journal of Geophysical Research 90, 12623–12632.
Forte, A.M., Perry, H.K.C., 2000. Geodynamic evidence for a chemically depleted continental tectosphere. Science 290, 1940–1944.
Foulger, G.R., Pritchard, M.J., Julian, B.R., Evans, J.R., Allen, R.M., Nolet, G., Morgan, W.J., Bergsson, B.H., Erlendsson, P., Jacobsdottir, S., Ragnarsson, S., Stefansson, R., Volgfjord, K., 2000. The seismic anomaly beneath Iceland extends down to the mantle transition zone and no deeper. Geophysical Journal International 142, F1–F5.
Francois, T., Burov, E., Meyer, B., Agard, P., in press. Survival and rheological structure of cratons: key constraints from surface topography. Tectonophysics. http://dx.doi.org/10.1016/j.tecto.2012.10.009.
Gale, S., 1992. Long-term landscape evolution in Australia. Earth Surface Processes and Landforms 17, 323–343.
Garcia-Castellanos, D., Cloetingh, S., 2012. Modeling the interaction between lithospheric and surface processes in foreland basins. In: Busby, C., Azor, A. (Eds.), Recent Advances, Tectonics of Sedimentary Basins. Wiley-Blackwell, pp. 152–184.
Garcia-Castellanos, D., Verges, J., Gaspar-Escribano, J., Cloetingh, S., 2003. Interplay between the tectonics, climate, and fluvial transport during the Cenozoic evolution of the Ebro Basin (NE Iberia). Journal of Geophysical Research 108, 2347.
Gerbault, M., Poliakov, A.N.B., Daignières, M., 1998. Prediction of faulting from the theories of elasticity and plasticity; what are the limits? Journal of Structural Geology 20, 301–320.
Gerbault, M., Burov, E., Poliakov, A., Dagnieres, M., 1999. Do faults trigger folding in the asthenosphere? Geophysical Research Letters 262, 271–274.
Gerya, T., 2010. Introduction to Numerical Geodynamic Modelling. Cambridge University Press (345 pp.).
Gerya, T., 2011. Future directions in subduction modeling. Journal of Geodynamics 52, 344–378.
Ghorbal, B., Bertotti, G., Foeken, J., Andriessen, P., 2008. Unexpected Jurassic to Neogene vertical movements in "stable" parts of NW Africa revealed by low temperature geochronology. Terra Nova 20, 355–363.
Goes, S., Spakman, W., Bijwaard, H., 1999. A lower mantle source for central European volcanism. Science 286, 1928–1931.
Gölke, M., Coblentz, D.D., 1996. Origin of the European regional stress field. Tectonophysics 266, 11–24.
Grand, S.P., 2002. Mantle shear wave tomography and the fate of subducted slabs. Philosophical Transactions of the Royal Society of London. Series A 360, 2475–2491.
Granet, M., Wilson, M., Achauer, U., 1995. Imaging mantle plumes beneath the French Massif Central. Earth and Planetary Science Letters 136, 199–203.
Griffin, W.L., O'Reilly, S.Y., Abea, N., Aulbach, S., Davies, R.M., Pearson, N.J., Doyle, B.J., Kivi, K., 2003. The origin and evolution of Archean lithospheric mantle. Precambrian Research 127, 19–41.
Guest, B., Guest, A., Axen, G., 2007. Late Tertiary tectonic evolution of northern Iran: a case for simple crustal folding. Global and Planetary Change 58, 435–453.
Guillou-Frottier, L., Jaupart, C., 1995. On the effects of continents on mantle convection. Journal of Geophysical Research 100, 24217–24238.
Guillou-Frottier, L., Burov, E., Nehlig, P., Wyns, R., 2007. Deciphering plume–lithosphere interactions beneath Europe with topographic signatures. Global and Planetary Change 58, 119–140.
Guillou-Frottier, L., Burov, E., Cloetingh, S., Le Goff, E., Deschamps, Y., Huet, B., Bouchot, V., 2012. Plume-induced dynamic instabilities near cratonic blocks: implications for P–T–t paths and metallogeny. Global and Planetary Change 90–91, 37–50.
Gung, Y., Panning, M., Romanowicz, B., 2003. Global anisotropy and the thickness of continents. Nature 422, 707–711.
Hammer, P.T.C., Clowes, R.M., Cook, F.A., van der Velden, A.J., Vasudevan, K., 2010. The Lithoprobe trans-continental lithospheric cross sections: imaging the internal structure of the North American continent. Canadian Journal of Earth Sciences 47, 821–857.
Horváth, F., Cloetingh, S., 1996. Stress-induced late-stage subsidence anomalies in the Pannonian basin. Tectonophysics 266, 287–300.
Horváth, F., Bada, G., Szafián, P., Tari, G., Adám, A., Cloetingh, S., 2006. Formation and deformation of the Pannonian basin: constraints from observational data. Geological Society of London, Memoirs 32, 207–221.
Houseman, C.A., Molnar, P., 1997. Gravitational (Rayleigh–Taylor) instability of a layer with nonlinear viscosity and convergence thinning of continental lithosphere. Geophysical Journal International 128, 125–150.
Houseman, G.A., McKenzie, D.P., Molnar, P., 1981. Convective instability of a thickened boundary layer and its relevance for the thermal evolution of continental convergent belts. Journal of Geophysical Research 86, 6115–6132.

Hunt, G., Muhlhaus, H., Hobbs, B., Ord, A., 1996. Localized folding of viscoelastic layers. Geologische Rundschau 85, 58–64.
Jackson, J., 2002. Strength of the continental lithosphere: time to abandon the jelly sandwich? GSA Today 12, 4–10.
Jarosiński, M., Beekman, F., Bada, G., Cloetingh, S., 2007. Redistribution of recent collision push and ridge push in Central Europe: insights from FEM modelling. Geophysical Journal International 167, 860–880.
Jaupart, C., Mareschal, J.C., 2007. Heat Flow and Thermal Structure of the Lithosphere. Treatise on Geophysics. Elsevier.
Jordan, T.H., 1981. Continents as a chemical boundary layer. Philosophical Transactions of the Royal Society of London, Series A 301, 359–373.
Katayama, I., Parkinson, C.D., Okamoto, K., Maruyama, S., Nakajima, Y., 1999. Ca-Eskola pyroxene in deeply subducted crustal rocks: evidence from the Kakchetav massif, Kazakhstan. EOS. Transactions of the American Geophysical Union 80, 176.
Katayama, I., Karato, S.-I., Brandon, M., 2005. Evidence for high water content in the deep upper mantle inferred from deformation microstructures. Geology 33, 613–616.
Kaus, B.J.P., 2010. Factors that control the angle of shear bands in geodynamic numerical models of brittle deformation. Tectonophysics 484, 36–47.
Keefner, J.W., Mackwell, S.J., Kohlstedt, D.L., Heidelbach, F., 2011. Dependence of dislocation creep of dunite on oxygen fugacity: implications for viscosity variations in Earth's mantle. Journal of Geophysical Research 116, B05201.
Kennett, B.L.N., Iaffaldano, G., 2013. Role of lithosphere in intra-continental deformation: Central Australia. Gondwana Research 24, 958–968 (this volume).
Kirby, S.H., Kronenberg, A.K., 1987. Rheology of the lithosphere: selected topics. Reviews of Geophysics 25, 1219–1244.
Kohlstedt, D.L., Evans, B., Mackwell, S.J., 1995. Strength of the lithosphere: constraints imposed by laboratory experiments. Journal of Geophysical Research 100, 17587–17602.
Kopylova, M.G., Russell, J.K., 2000. Chemical stratification of cratonic lithosphere: constraints from the Northern Slave craton, Canada. Earth and Planetary Science Letters 181, 71–87.
Koulakov, I., Kaban, M.K., Tesauro, M., Cloetingh, S., 2009. P- and S-velocity anomalies in the upper mantle beneath Europe from tomographic inversion of ISC data. Geophysical Journal International 179, 345–366.
Lavier, L.L., Steckler, M.S., 1997. The effect of sedimentary cover on the flexural strength of the continental lithosphere. Nature 389, 476–479.
Lefort, J.P., Agarwal, B.N.P., 1996. Gravity evidence for an Alpine buckling of the crust beneath the Paris Basin. Tectonophysics 258, 1–14.
Lefort, J.P., Agarwal, B.N., 2000. Gravity and geomorphological evidence for a large crustal bulge cutting across Brittany (France): a tectonic response to the closure of the Bay of Biscay. Tectonophysics 323, 149–162.
Lefort, J.P., Agarwal, B.N., 2002. Topography of the Moho undulations in France from gravity data: their age and origin. Tectonophysics 350, 193–213.
Lenardic, A., Moresi, L.N., Mühlhaus, H., 2003. Longevity and stability of cratonic lithosphere: insights from numerical simulations of coupled mantle convection and continental tectonics. Journal of Geophysical Research B, Solid Earth and Planets 108, 2303.
Lévy, F., Jaupart, C., 2011. Temperature and rheological properties of the mantle beneath the North American craton from an analysis of heat flux and seismic data. Journal of Geophysical Research 116, B01408.
Lévy, F., Jaupart, C., Mareschal, J.-C., Bienfait, G., Limare, A., 2010. Low heat flux and large variations of lithospheric thickness in the Canadian Shield. Journal of Geophysical Research 115, B06404.
Lithgow-Bertelloni, C., Richards, M.A., 1998. The dynamics of Cenozoic and Mesozoic plate motions. Reviews of Geophysics 36, 27–78.
Lustrino, M., Carminati, E., 2007. Phantom plumes in Europe and the circum-Mediterranean region. Geological Society of America Special Paper 430, 723–745.
MacKenzie, J.M., Canil, D., 1999. Composition and thermal evolution of cratonic mantle beneath the central Archean Slave Province, NWT, Canada. Contributions to Mineralogy and Petrology 134, 313–324.
Mackwell, S.J., Zimmerman, M.E., Kohlstedt, D.L., 1998. High-temperature deformation of dry diabase with applications to tectonics on Venus. Journal of Geophysical Research 103, 975–984.
Mareschal, J.-C., Jaupart, C., 2004. Variations of surface heat flow and lithospheric thermal structure beneath the North American craton. Earth and Planetary Science Letters 223, 65–77.
Martinod, J., Davy, P., 1992. Periodic instabilities during compression or extension of the lithosphere: 1. Deformation modes from an analytical perturbation method. Journal of Geophysical Research 97, 1999–2014.
Martinod, J., Davy, P., 1994. Periodic instabilities during compression of the lithosphere: 2. Analogue experiments. Journal of Geophysical Research 99, 12057–12069.
McKenzie, D.P., 1978. Some remarks on the development of sedimentary basins. Earth and Planetary Science Letters 95, 53–72.
McKenzie, D.P., Fairhead, J.D., 1997. Estimates of the effective elastic thickness of the continental lithosphere from Bouguer and free-air gravity anomalies. Journal of Geophysical Research 102, 27523–27552.
McNutt, M.K., Diament, M., Kogan, M.G., 1988. Variation of elastic plate thickness at continental thrust belts. Journal of Geophysical Research 93, 8825.
Missenard, Y., Zeyen, H., Frizon de Lamotte, D., Leturmy, P., Petit, C., Sébrier, M., Saddiqi, O., 2006. Crustal versus asthenospheric origin of relief of the Atlas Mountains of Morocco. Journal of Geophysical Research 111, B03401.
Mitrovica, J.X., Beamont, C., Jarvis, G.T., 1989. Tilting of continental interiors by the dynamical effects of subduction. Tectonics 8, 1079–1094.
Montelli, R., Nolet, G., Dahlen, F.A., Masters, G., Engdahl, E.R., Hung, S.H., 2004. Finite-frequency tomography reveals a variety of plume in the mantle. Science 303, 338–343.
Naylor, M., Sinclair, H.D., 2008. Pro- vs. retro foreland basins. Basin Research 20, 1365–2117.
Nyblade, A.A., Sleep, N.H., 2003. Long lasting epeirogenic uplift from mantle plumes and the origin of the Southern African Plateau. Geochemistry, Geophysics, Geosystems 4, 1105.
Parsons, B., Sclater, J.G., 1977. An analysis of the variation of ocean floor bathymetry and heat flow with age. Journal of Geophysical Research 82, 803–827.
Pérez-Gussinyé, M., Watts, A.B., 2005. The long-term strength of Europe and its implications for plate forming processes. Nature 436, 381–384.
Pilidou, S., Priestley, K., Debayle, E., Gudmundsson, O., 2005. Rayleigh wave tomography in the North Atlantic: high resolution images of the Iceland, Azores and Eifel mantle plumes. Lithos 79, 453–474.
Pitman, W.C., Golovchenko, X., 1983. The effect of sealevel change on the shelf edge and slope of passive margin. In: Stanlay, D.J., Moore, G.T. (Eds.), The Shelf Break: Critical Interface on Continental Margins: SEPM Spec. Publ., 33, pp. 41–58.
Poliakov, A.N.B., Cundall, P., Podladchilov, Y., Laykhovsky, V., 1993. An explicit inertial method for the simulation of visco-elastic flow: an evaluation of elastic effects on diapiric flow in two- or three-layers models. In: Stone, D.B., Runcorn, S.K. (Eds.), Flow and Creep in the Solar System: Observations, Modelling and Theory: Dynamic Modelling and Flow in the Earth and Planet Series, pp. 175–195.
Poudjom Djomani, Y.H., O'Reilly, S.Y., Griffin, W.L., Morgan, P., 2001. The density structure of subcontinental lithosphere through time. Earth and Planetary Science Letters 184, 605–621.
Ramberg, H., 1961. Contact strain and folding instability of multilayered body under compression. Geologische Rundschau 51, 405–439.
Ranalli, G., 1995. Rheology of the Earth, second ed. Chapman and Hall, London (413 pp.).
Ranalli, G., Murphy, D.C., 1987. Rheological stratification of the lithosphere. Tectonophysics 132, 281–295.
Ribe, N.M., Christensen, U.R., 1994. Three-dimensional modeling of plume–lithosphere interaction. Journal of Geophysical Research 99, 669–682.
Ritter, J.R.R., 2005. Small-scale mantle plumes: imaging and geodynamic aspects. In: Wenzel, F. (Ed.), Perspectives in Modern Geology. Lectures Notes in Earth Sciences, 105. Springer Verlag, Heidelberg, pp. 69–94.
Ritter, J.R.R., Jordan, M., Christensen, U.R., Achauer, U., 2001. A mantle plume below the Eifel volcanic fields, Germany. Earth and Planetary Science Letters 186, 7–14.
Ritzmann, O., Faleide, J.I., 2009. The crust and mantle lithosphere in the Barents Sea/Kara Sea region. Tectonophysics 470, 89–104.
Romanowicz, B., Gung, Y.C., 2002. Superplumes from the core–mantle boundary to the base of the lithosphere. Science 296, 513–516.
Roure, F., Cloetingh, S., Scheck-Wenderoth, M., Ziegler, P.A., 2010. Achievements and challenges in sedimentary basin dynamics: a review. In: Cloetingh, S., Negendank, J. (Eds.), New Frontiers in Integrated Solid Earth Sciences. Springer-Verlag, Berlin, pp. 145–233.
Royden, L., 1988. Flexural behaviour of the continental lithosphere in Italy: constraints imposed by gravity and deflection data. Journal of Geophysical Research 93, 7747–7766.
Rychert, C.A., Shearer, P.M., 2009. A global view of the lithosphere–asthenosphere boundary. Science 324, 495–498.
Schmeling, H., Babeyko, A., Enns, A., Faccenna, C., Funiciello, F., Gerya, T., Golabek, G., Grigull, S., Kaus, B., Morra, G., van Hunen, J., 2008. A benchmark comparison of spontaneous subduction models — towards a free surface. Physics of the Earth and Planetary Interiors 171, 198–223.
Schubert, G., Turcotte, D.L., Olson, P., 2001. Mantle Convection in the Earth and Planets. Cambridge University Press, p. 956.
Shapiro, N.M., Ritzwoller, M.H., 2002. Monte Carlo inversion for a global shear wave velocity model of the crust and upper mantle. Geophysical Journal International 151, 88–105.
Shapiro, S.S., Hager, B.H., Jordan, T.H., 1999. Stability and dynamics of the continental tectosphere. Lithos 48, 115–133.
Sleep, N.H., 2003a. Survival of Archean cratonal lithosphere. Journal of Geophysical Research 108, 2302.
Sleep, N.H., 2003b. Fate of mantle plume material trapped within a lithospheric catchment with reference to Brazil. Geochemistry, Geophysics, Geosystems 4, 8509.
Smit, J.H.W., Cloetingh, S.A.P.L., Burov, E., Tesauro, M., Sokoutis, D., Kaban, M., in press. Interference of lithospheric folding in western Central Asia by simultaneous Indian and Arabian plate indentation. Tectonophysics. http://dx.doi.org/10.1016/j.tecto.2012.10.032.
Smith, R.B., 1979. The folding of a strongly non-Newtonian layer. American Journal of Science 79, 272–287.
Sokoutis, D., Burg, J.P., Bonini, M., Corti, G., Cloetingh, S., 2005. Lithospheric-scale structures from the perspective of analogue continental collision. Tectonophysics 406, 1–15.
Solomatov, V.S., 1995. Scaling of temperature- and stress-dependent viscosity convection. Physics of Fluids 7, 266–274.
Solomatov, V.S., Moresi, L.N., 2000. Scaling of time-dependent stagnant lid convection; application to small-scale convection on Earth and other terrestrial planets. Journal of Geophysical Research 105, 21795–21817.
Stephenson, R.A., Cloetingh, S., 1991. Some examples and mechanical aspects of continental lithospheric folding. Tectonophysics 188, 27–37.
Stephenson, R.A., Lambeck, K., 1985. Isostatic response of the lithosphere with in-plane stress: application to Central Australia. Journal of Geophysical Research 90, 8581–8588.
Stephenson, R.S., Ricketts, B.D., Cloetingh, S., Beekman, F., 1990. Lithosphere folds in the Eurekan orogen, Arctic Canada? Geology 18, 603–606.
Tarapoanca, M., Bertotti, G., Matenco, L., Dinu, C., Cloetingh, S., 2003. Architecture of the Focsani depression: a 13 km deep basin in the Carpathians bend zone (Romania). Tectonics 22, 1074.
Tesauro, M., Kaban, M., Cloetingh, S., Hardebol, N., Beekman, F., 2007. 3D strength and gravity anomalies of the European lithosphere. Earth and Planetary Science Letters 263, 56–73.

Tesauro, M., Kaban, M., Cloetingh, S., 2012a. Global strength and elastic thickness of the lithosphere. Global and Planetary Change 90–91, 51–57.
Tesauro, M., Audet, P., Kaban, M.K., Burgmann, R., Cloetingh, S., 2012b. The effective elastic thickness of the continental lithosphere: comparison between rheological and inverse approaches. Geochemistry, Geophysics, Geosystems 13, Q09001.
Thomas, J.C., Cobbold, P.R., Shein, V.S., Le Douaran, S., 1999a. Sedimentary record of late Paleozoic to Recent tectonism in central Asia: analysis of subsurface data from the Turan and south Kazak domains. Tectonophysics 313, 243–263.
Thomas, J.C., Grasso, J.R., Bossu, R., Martinod, J., Nurtaev, B., 1999b. Recent deformation in the Turan and South Kazakh platforms, western central Asia, and its relation to Arabia–Asia and India–Asia collisions. Tectonics 18, 201–214.
Toussaint, G., Burov, E., Jolivet, L., 2004. Continental plate collision: unstable vs. stable slab dynamics. Geology 32, 33–36.
Trompert, R., Hansen, U., 1998. Mantle convection simulations with rheologies that generate plate-like behaviour. Nature 395, 686–689.
Turcotte, D.L., Schubert, G., 2002. Geodynamics, Applications of Continuum Physics to Geological Problems, second ed. Cambridge Univ. Press (456 pp.).
Van Wees, J.D., Van Bergen, F., David, P., Nepveu, M., Beekman, F., Cloetingh, S., 2009. Probabilistic tectonic heat flow modelling for basin maturation: method and applications. Marine and Petroleum Geology 26, 536–551.
Watts, A.B., 2001. Isostasy and Flexure of the Lithosphere. Cambridge University Press, Cambridge (458 pp.).
Watts, A.B., Burov, E.B., 2003. Lithospheric strength and its relationship to the elastic and seismogenic thickness. Earth and Planetary Science Letters 213, 113–131.
White, N., Lovell, B., 1997. Measuring the pulse of a plume with the sedimentary record. Nature 387, 888–891.
Wilks, K.R., Carter, N.L., 1990. Rheology of some continental lower crustal rocks. In: Fountain, D.M., Boriani, A. (Eds.), The Nature of the Lower Continental Crust: Tectonophysics, 182, pp. 57–77.
World Stress Map, 2007. World Stress Map. URL: http://www.world-stress-map.org/.
Wortel, M.J.R., Spakman, W., 2000. Subduction and slab detachment in the Mediterranean–Carpathian region. Science 290, 1910–1917.
Xu, Y.G., 2001. Thermo-tectonic destruction of the Archean lithospheric keel beneath the sino-korean craton in china: evidence, timing and mechanism. Physics and Chemistry of the Earth 26, 747–757.
Yamato, P., Agard, P., Burov, E., Le Pourhiet, L., Jolivet, L., Tiberi, C., 2007. Burial and exhumation in a subduction wedge: mutual constraints from thermo-mechanical modelling and natural p–t–t data (sch. Lustres, w. Alps). Journal of Geophysical Research 112, B07410.
Yamato, P., Burov, E., Agard, P., Le Pourhiet, L., Jolivet, L., 2008. HP-UHP exhumation processes during continental subduction (W. Alps): when thermomechanical models reproduce P-T-t data. Earth and Planetary Science Letters 271, 63–75.
Ziegler, P.A., Dèzes, P., 2007. Neogene uplift of Variscan Massifs in the Alpine foreland: timing and controlling mechanisms. Global and Planetary Change 58, 237–269.
Ziegler, P.A., Van Wees, J.-D., Cloetingh, S.A.P.L., 1998. Mechanical controls on collision-related compressional intraplate deformation. Tectonophysics 300, 103–129.
Zoetemeijer, R., Cloetingh, S., Sassi, W., Roure, F., 1993. Modelling of piggy-back basin stratigraphy: record of tectonic evolution. Tectonophysics 226, 253–269.
Zoetemeijer, R., Tomek, C., Cloetingh, S., 1999. Flexural expression of European continental lithosphere under the western outer Carpathians. Tectonics 18, 843–861.